5
Heat Management by Microdevices

This chapter is devoted to the discussion of thermal effects during chemical reactions with the main emphasis on how they can be controlled by using microdevices. A short introduction outlines the basic principles used in chemical reaction engineering without going into the details of thermostability of conventional flow reactors. The reader can find these topics in general text books on conventional chemical reactor design and engineering.

5.1
Introduction

Nearly all chemical reactions are accompanied by heat production or heat consumption. Therefore, strictly isothermal conditions are hard to attain in chemical reactors. Consequently, heat effects must be taken into account when evacuating or supplying heat to the reaction mixture. In general, a certain temperature range is specified in which the reactions have to be carried out in order to assure safe operation and to reach the desired product yield and selectivity at acceptable reactor performance.

Different factors influence the choice of the temperature range for the chemical transformations, such as

- The physical properties of the reaction mixture (boiling point, melting point, viscosity, etc.).
- The thermodynamics and kinetics, such as chemical equilibrium, importance of side reactions, and their temperature dependencies.
- The temperature stability of eventually used homogeneous or heterogeneous catalysts.
- The cost related to heating up the reaction mass and to keep the temperature at the prescribed level.

There are several means to facilitate the heat management of chemical reactors, such as

- Adjusting the inlet temperature.

Microstructured Devices for Chemical Processing, First Edition.
Madhvanand N. Kashid, Albert Renken and Lioubov Kiwi-Minsker.

- Adding inert compounds (solvents) to reduce the reactant concentration and in consequence the heat production rate and adiabatic temperature rise.
- Increasing the heat conductivity of the reactor material and/or of the catalytic or inert packing in the reactor.

The final choice between these options and the design of the chemical reactor are always based on the properly applied relations between mass and heat balances.

As pointed out in Chapter 2, the design of chemical reactors is based on material and energy balances. The balances are established for a small volume of the system. For an unambiguous description, the system volume is chosen in such a way that concentrations and temperature can be considered as uniform. A material balance needs to be set up for all species participating in the reactions within the reactor. For a component A_i the material balance can be formulated in the following manner:

$$\begin{Bmatrix}\text{accumulation of } A_i \text{ in the system element}\end{Bmatrix} = \begin{Bmatrix}\text{rate of flow of } A_i \text{ into the element}\end{Bmatrix} - \begin{Bmatrix}\text{rate of flow of } A_i \text{ out of the element}\end{Bmatrix} + \begin{Bmatrix}\text{rate of production or disappearance of } A_i \text{ in the system element}\end{Bmatrix} \tag{5.1}$$

$$\frac{dn_i}{dt} = \dot{n}_{i,0} - \dot{n}_i + P_i$$

where n_i represents the number of moles of species A_i in the system at time t, $\dot{n}_i$ is the molar flow rate, and P_i is the rate of A_i production or disappearance. The last term in the above equation is often referred to as *source term*, which is the basis of reaction engineering fundamentals. The rate of A_i production corresponds to the product of system volume, ΔV, and the transformation rate, R_i of A_i (see Chapter 2).

$$P_i = R_i \cdot \Delta V \tag{5.2}$$

With the exception of special cases, it is generally sufficient to limit the energy balance for chemical reactors to a heat balance.

$$\begin{Bmatrix}\text{rate of heat accumulation within the system element}\end{Bmatrix} = \begin{Bmatrix}\text{rate of energy added to the system by convection}\end{Bmatrix} - \begin{Bmatrix}\text{rate of energy leaving the system by convection}\end{Bmatrix} + \begin{Bmatrix}\text{rate of heat exchanged with the surroundings}\end{Bmatrix} + \begin{Bmatrix}\text{heat generated by reaction in the system element}\end{Bmatrix} \tag{5.3}$$

$$\frac{dQ}{dt} = \dot{Q}_{c,0} - \dot{Q}_c + \dot{Q}_{ex} + \dot{Q}_r$$

Chemical reactors are generally modeled using continuum assumption meaning that space and time are parts of the same continuum rather than as separate entities. Because of the small size of microstructured reactors (MSR), one has to investigate whether a model of continuous and indefinitely divisible matter is still valid at a channel size as low as 100 µm. For gases, continuum models can be used to describe a system as long as the mean free path of molecules λ' is much smaller than the characteristic length of the MSR (l_char). A criterion is defined on the base of the Knudsen coefficient, *Kn,* which is given as follows

$$Kn = \frac{\lambda'}{l_\mathrm{char}} \tag{5.4}$$

Following [1] the continuum assumptions in microstructured devices are valid for $Kn < 10^{-3}$.

For a gas phase under atmospheric pressure at 298 K, the mean free path of an air molecule corresponds to $\lambda' = 6.7 \times 10^{-8}$ m [2]. In this case, the system can be modeled with the continuum equations down to a characteristic size of l_{char} =67 µm. As for an ideal gas λ' is proportional to T and p^{-1}, the modeling of small reactors at high temperatures or low pressures can become critical. In liquid systems, describing the limits to non-Newtonian behavior is more problematic. The boundary can be approximated as [3]:

$$\dot{\gamma} = \frac{\partial u}{\partial z} \geq \frac{2}{\tau'} \tag{5.5}$$

With the shear rate $\dot{\gamma}$, and

$$\tau' = \left(\frac{m \cdot \sigma^2}{\epsilon} \right)^{0.5} \tag{5.6}$$

where τ' is the molecular time scale (s), m is the molecular mass (kg), σ is the molecular length (m), and ϵ the molecular energy scale (J). For water at standard temperature and pressure ($T = 273.15$ K, $p = 10^5$ Pa) $\tau' = 8.31 \cdot 10^{-13}$ s. In this case, only very high shear rates would cause continuum assumption to fail. Experimental results given in the literature predict a Newtonian behavior down to films of 10 molecular layers for nonpolar molecules and to characteristic lengths <1 µm for polar molecules [4–6]. Therefore, the assumption of continuous and indefinitely divisible matter is valid for liquids in nearly all cases.

5.2
Heat Transfer in Microstructured Devices

5.2.1
Straight Microchannels

If the locally produced or consumed heat by chemical reaction is different from the locally evacuated or supplied heat, isothermal operation is impossible and axial temperature profiles will develop leading to locally higher or lower temperatures compared to the cooling/heating medium. So-called hots pots or cold spots will be observed. As mentioned above, the developed temperature profile in chemical reactors is of crucial importance for the obtainable product selectivity, yield, and productivity. Therefore, high heat transfer performances are important to keep the temperature within a defined narrow range.

In microstructured tubular reactors, the heat is generally evacuated or supplied by maintaining constant temperature of the cooling medium (T_c). The heat transfer performance of the system depends on the overall heat transfer coefficient (U) and exchange surface (A).

$$\dot{Q} = U \cdot A(T_c - T) \quad \text{with } T : \text{the temperature of the reacting fluid} \tag{5.7}$$

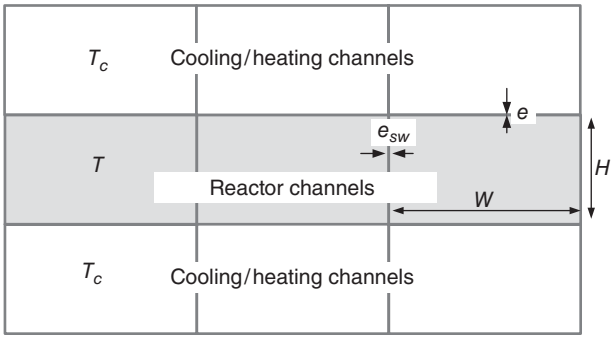

Figure 5.1 Parallel arrangement of cooling and reactor channels.

The overall heat transfer coefficient includes all the resistances to the evacuation of heat, that is, the resistance between channel wall and the reacting fluid h_r, the channel wall itself h_{wall} and the resistance located in the cooling fluid h_c [7]. For parallel arranged microchannels as shown in Figure 5.1 the overall heat transfer coefficient for the rectangular channels is given by the following equation:

$$\frac{1}{U} = \frac{1}{h_r} + \frac{1}{h_{\text{wall}}} + \frac{1}{h_c} = \frac{1}{h_r} + \frac{e}{\lambda_{\text{wall}}} + \frac{1}{h_c} \tag{5.8}$$

where e is the wall thickness of the channels and λ_{wall} the heat conductivity of the wall material.

Because of the small channel diameters of the microchannels, laminar flow can be considered. The radial velocity profile in the channels develops from the entrance to the position where a complete Poiseuille profile is established. The length of the entrance zone depends on the *Re* and the channel diameter. In a similar way, radial temperature profiles develop. This is schematically shown in Figure 5.2.

Within the entrance zone the heat transfer coefficient diminishes, reaching an asymptotic value. The dependency for constant wall temperature can be described in terms of the *Nusselt numbers* [8]

$$Nu = \frac{h \cdot d_h}{\lambda_f} \tag{5.9}$$

where λ_f is the thermal conductivity of the fluid and d_h the hydraulic diameter of the channel.

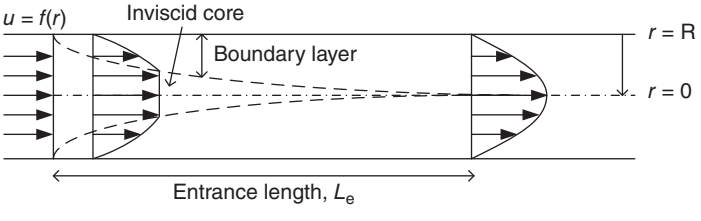

Figure 5.2 Development of laminar velocity profile (schematic).

Table 5.1 Values of Nu_∞, Sh_∞ for different geometries and constant wall temperature [9].

Geometry	Nu_∞, Sh_∞
Circular	3.66
Ellipse (width/height = 2)	3.74
Parallel plates	7.54
Rectangle (height/width = 0.25)	4.44
Rectangle (height/width = 0.5)	3.39
Square	2.98
Equilateral triangle	2.47
Sinusoidal	2.47
Hexagonal	3.66

For laminar flow and completely developed radial velocity and temperature profiles the local heat transfer is constant and the mean Nusselt number reaches an asymptotic value, given by Nu_∞. The same value is obtained for the asymptotic Sherwood number, Sh_∞ characterizing the mean mass transfer between the fluid and the channel wall (see Chapter 6).

The asymptotic Nusselt and Sherwood numbers depend on the geometry of the channel as summarized in Table 5.1.

For simultaneously developing radial velocity and temperature profiles, the thickness of the boundary layers increase with increasing distance from the entrance of the channel. As a consequence, the local heat transfer diminishes until the profile is completely developed. The mean *Nu* over the channel length depends on the ratio, d_h/L_t, the Reynolds, *Re,* and the Prandtl number, *Pr.*

$$Nu_m = f\left(Re \cdot Pr \cdot \frac{d_h}{L_t}\right); \quad Pr = \frac{\nu}{\alpha} = \frac{\mu c_p}{\lambda}; \quad Re = \frac{u \cdot d_h}{\nu} \tag{5.10}$$

with $\alpha = \rho \cdot c_p/\lambda$, the thermal diffusivity.

The following empirical relation describes the mean *Nu* for all lengths, L_t of the tubular reactor at constant wall temperature [8]:

$$Nu_m = \left[Nu_\infty^3 + 0.7^3 + \left(Nu_2 - 0.7\right)^3 + Nu_3^3\right]^{\frac{1}{3}} \tag{5.11}$$

with

$$Nu_2 = 1.615\left(Re \cdot Pr \cdot \frac{d_h}{L_t}\right)^{\frac{1}{3}} \tag{5.12}$$

$$Nu_3 = \left(\frac{2}{1 + 22Pr}\right)^{\frac{1}{6}} \left(Re \cdot Pr \cdot \frac{d_h}{L_t}\right)^{\frac{1}{2}} \tag{5.13}$$

The mean *Nu* as function of $\left(Re \cdot Pr \cdot \frac{d_h}{L_t}\right)$ is shown in Figure 5.3 for a concentric channel and $Pr = 6$.

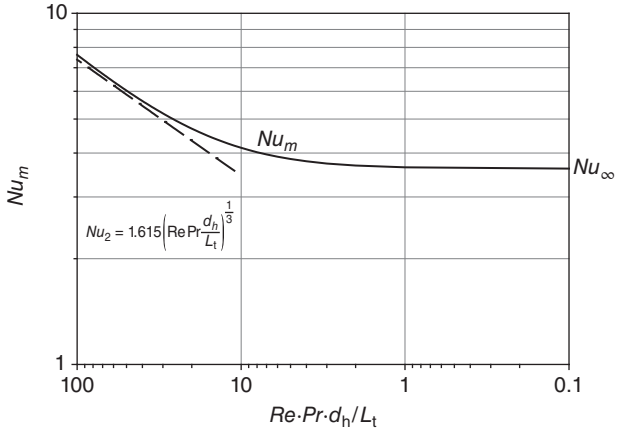

Figure 5.3 Mean Nusselt number as function of $(Re{\cdot}Pr{\cdot}d_h/L_t)$ $(Pr = 6)$.

As can be seen on Figure 5.3, the *Nu*-number for short channels and/or high *Re* $(Re \cdot Pr \cdot d_h/L_t) \geq 20$ can be estimated with Equation 5.12. For long channels and/or low *Re* corresponding to $(Re \cdot Pr \cdot d_h/L_t) < 20$ the asymptotic *Nu* can be used as good approximation $(Nu_m \cong Nu_\infty)$.

If reactor and cooling channels are arranged in an alternate fashion, only two sides are in direct contact with the cooling channels. If the side walls between the adjacent reactor channels are small compared to the channel width and height $(e_{sw} \ll W, H)$ the walls can be considered as adiabatic and do not contribute to the heat evacuation (see Figure 5.1). The active heat exchange area between the reaction and the cooling channels A_{HEX} is given by the width and the length of the channel. For N parallel channels follows:

$$A_{HEX} = N \cdot W \cdot L_t \text{ (cooling on one side)} \tag{5.14}$$

The heat exchange area has to be doubled, if the reaction channels are situated between two cooling channels as indicated in Figure 5.1.

The radial temperature profile in channels with only two active walls is different compared to channels surrounded by the cooling medium, where all four sides contribute to the heat exchange. This in turn influences the asymptotic *Nu* as shown in Figure 5.4 [10]. The upper curve corresponds to rectangular channels with only two walls cooled/heated, whereas the lower curve shows Nu_∞ for ducts with all walls available for heat exchange. It is important to note that Nu_∞ and, therefore, the heat transfer coefficient increases with decreasing aspect ratio. The highest values are found for $H/W \to 0$ corresponding to microchannels in the form of small slits.

If only one side of the reaction channel is in contact with the cooling channel as shown in Figure 5.7, a further reduction of the asymptotic *Nu* is observed, and even for parallel plates the heat transfer coefficient is roughly half of the value obtained in channels with two–four cooling walls (see Example 5.1).

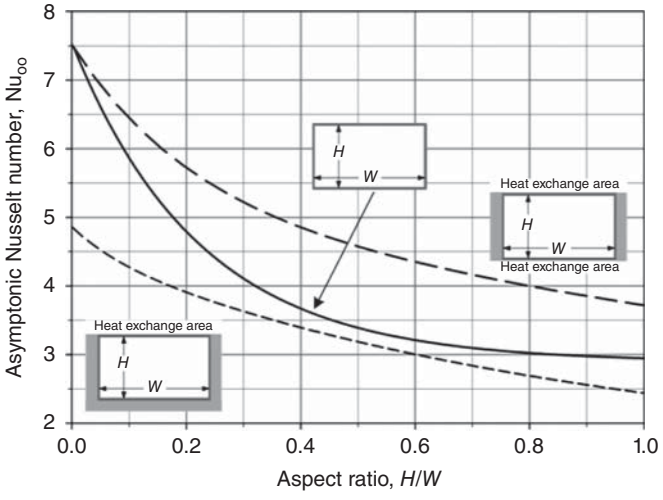

Figure 5.4 Values of the asymptotic Nusselt -number as function of the aspect ratio for 1, 2, and 4 walls cooled/heated. (Values taken from Ref. [10].)

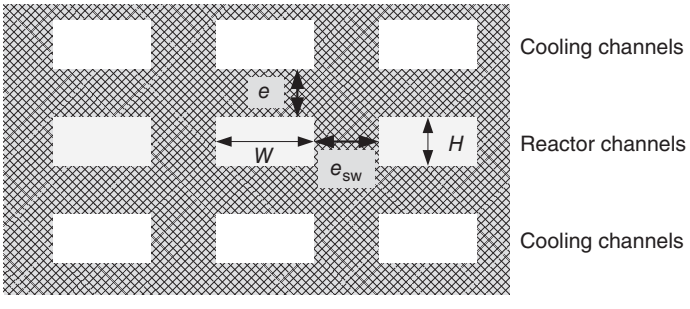

Figure 5.5 Parallel arranged cooling and reactor channels with thick channel walls.

In MSR with relatively thick walls (Figure 5.5), adiabatic behavior between two adjacent channels cannot be assumed. In this case, the walls between the channels contribute to the heat exchange and must be included partially in the heat exchange area. The resulting effective exchange area is estimated by including the heat conductivity in the side walls with the thickness e_{sw}. A way to estimate the effective heat exchange area between cooling and reaction channels was proposed in [11, 12] for rectangular channels (Equation 5.15).

$$A_{\text{eff,ch}} = (W + \eta_{sw} H) \cdot L_t \text{ (one channel)} \tag{5.15}$$

The efficiency factor η_{sw} is defined as follows [11]:

$$\eta_{sw} = \frac{\tanh(\sqrt{2h_r/(\lambda_{wall} e_{sw})} \cdot H/2)}{\sqrt{2h_r/(\lambda_{wall} e_{sw})} \cdot H/2} \tag{5.16}$$

For the estimation of the efficiency factor, the heat transfer coefficient h_r has to be known. A rough estimation leads to the conclusion that in most practical situations, η_{sw} is between 0.8 and 1.

A more practical way to estimate the effective heat exchange area consists in considering the sum of the channel width and the wall thickness as shown in Equation 5.17.

$$A_{HEX} \cong (W + e_{sw}) \cdot L_t \tag{5.17}$$

Besides microstructured heat exchanger/reactors constructed in the form of plates as shown in Figure 5.1, shell and tube micro heat exchangers are available. An example is shown in Figure 5.6. The heat transfer within the reactor tubes can be estimated with the asymptotic *Nu* or with Equation 5.12 for short channels. The outer heat transfer coefficient depends on the flow regime, the arrangement of the tubes, and the presence of baffles [8, 13]. For small-scale systems, capillaries submerged in constant temperature baths are commonly used. In this case, the main heat transfer resistance is mostly located at the outer side of the reactor.

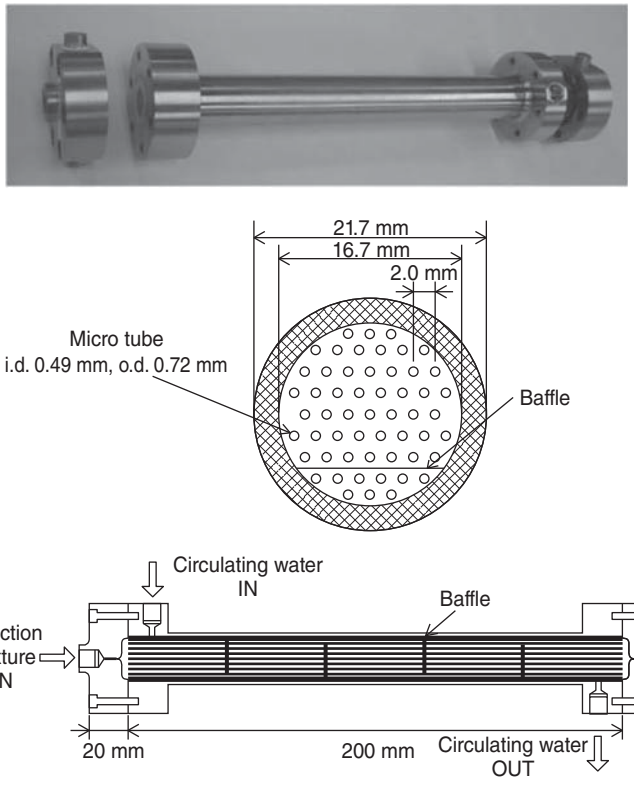

Figure 5.6 Shell and tube micro heat exchanger. (Reprinted with permission from Ref. [14]. Copyright (2005) American Chemical Society.)

Example 5.1: Heat transfer performance of a slit-like MSR.

Estimate the overall heat transfer coefficient (U) for a flow through microstructured reactor with a rectangular reaction and cooling channel (see Figure 5.7). The isolated device is constructed of stainless steel. The reaction is carried out in toluene as solvent; water is used as cooling fluid. Details are summarized in Tables 5.2 and 5.3.

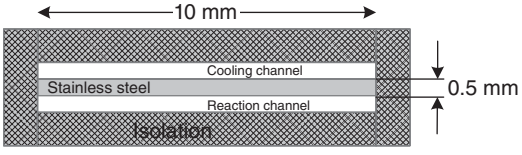

Figure 5.7 Cross section of the microstructured reactor.

Table 5.2 Reactor details.

Construction material	Stainless steel
Heat conductivity, λ_{ss} (W m^{-1} K^{-1})	21
Length, L_t (mm)	200
Channel-Width, W (mm)	10
Channel-Height, H (mm)	0.5

Table 5.3 Physical properties of the fluids.

	Water	Toluene
Density, ρ (kg m^{-3})	1000	867
Dynamic viscosity, μ (Pa s)	$1.0 \cdot 10^{-3}$	$0.58 \cdot 10^{-3}$
Heat capacity, c_p (kJ kg^{-1} K^{-1})	4.2	1.72
Heat conductivity, λ (W m^{-1} K^{-1})	0.6	0.141
Flow rate (inlet), $\dot{V}_0$ (l h^{-1})	9.0	0.36

Solution:

The hydrodynamic diameter of the reactor and the cooling channel are

$$d_h = \frac{4 \cdot A_{cs}}{L_{circ}} = \frac{4(H \cdot W)}{2(H + W)} = \frac{4 \cdot 0.5 \cdot 10}{2 \cdot (0.5 + 10)} = 0.95\,\text{mm}$$

The cross section area is $A_{cs} = 5{\cdot}10^{-6}$ m^2.
Flow regime in the two channels:

Reynolds number: $Re = \frac{u \cdot d_h}{\nu}$; $\nu = \frac{\mu}{\rho}$;

The mean velocity in the cooling channel is: $u_c = \frac{\dot{V}_0}{A_{cs}} = 0.5\,\mathrm{m\,s^{-1}}$

$Re_c = \frac{0.5 \cdot 0.95\,10^{-3}}{10^{-6}} = 475$ (laminar flow in the cooling channel)

The mean velocity in the reaction channel is: $u_r = \frac{\dot{V}_0}{A_{cs}} = 0.02\,\mathrm{m\,s^{-1}}$

$$Re_r = \frac{0.02 \cdot 0.95 \cdot 10^{-3}}{0.67 \cdot 10^{-6}} = 28$$

The flow regimes in both channels are laminar.

Heat transfer coefficient:

The heat transfer coefficient will be estimated on the basis of Figure 5.4. To use the asymptotic Nusselt number, Nu_∞, the group $Re{\cdot}Pr{\cdot}d_h/L_t$ should be lower than 20 (see Figure 5.3).

$$\left(Re \cdot Pr \cdot \frac{d_h}{L_t}\right) = \frac{\overline{u} \cdot d_h}{\alpha}\frac{d_h}{L_t} = \frac{\overline{u} \cdot d_h \cdot \rho c_p}{\lambda}\frac{d_h}{L_t}$$

$$\text{cooling channel}: \left(Re \cdot Pr \cdot \frac{d_h}{L_t}\right) = \frac{0.5 \cdot 0.95 \cdot 10^{-3} \cdot 1000 \cdot 4.2}{0.6 \cdot 10^{-3}}\frac{0.95 \cdot 10^{-3}}{0.2} = 15.8$$

$$\text{reaction channel}: \left(Re \cdot Pr \cdot \frac{d_h}{L_t}\right) = \frac{0.02 \cdot 0.95 \cdot 10^{-3} \cdot 867 \cdot 1.72}{0.141 \cdot 10^{-3}}\frac{0.95 \cdot 10^{-3}}{0.2} = 0.95$$

For both channels, Nu_∞ will be used for estimating the heat transfer coefficient. With the aspect ratio $H/W = 0.05$, we obtain from Figure 5.4, $Nu_\infty = 4.5$.

The heat transfer coefficient is given by $h = \frac{Nu_\infty \cdot \lambda_f}{d_h}$

$$\text{cooling channel}: h_c = \frac{4.5 \cdot 0.6}{0.95 \cdot 10^{-3}} = 2840\,\frac{\mathrm{W}}{\mathrm{m^2K}}$$

$$\text{reaction channel}: h_r = \frac{4.5 \cdot 0.141}{0.95 \cdot 10^{-3}} = 668\,\frac{\mathrm{W}}{\mathrm{m^2K}}$$

The overall heat transfer coefficient is estimated with Equation 5.8:

$$\frac{1}{U} = \frac{1}{h_r} + \frac{e}{\lambda_{\mathrm{wall}}} + \frac{1}{h_c} = \frac{1}{2840} + \frac{0.5 \cdot 10^{-3}}{21} + \frac{1}{668} = 1.873 \cdot 10^{-3}\,\frac{\mathrm{m^2K}}{\mathrm{W}}$$

$$\Rightarrow U = 534\frac{\mathrm{W}}{\mathrm{m^2K}}$$

For the overall volumetric heat transfer coefficient, U_v, follows:

$$U_v = U\frac{A_{\mathrm{ref}}}{V_R} = 534\frac{0.01 \cdot 0.2}{0.5 \cdot 10^{-3}0.01 \cdot 0.2} = 1.068 \cdot 10^6\,\frac{\mathrm{W}}{\mathrm{m^3K}} = 1.068\,\frac{\mathrm{MW}}{\mathrm{m^3K}}$$

5.2.2
Curved Channel Geometry

Heat transfer can be considerably enhanced by using zig-zag or periodically curved channels. Theoretical studies confirmed that in zig-zag channels significant increases of the *Nu* compared to straight channels can be obtained. For $Re = 1000$ and $Pr = 8$ (corresponding to water) one order of magnitude higher heat transfer coefficients were found. For $Pr = 0.7$ (corresponding to air) an increase by a factor of 6 can be obtained for the same pressure loss as in straight channels. This is an important observation in view of the design of high performance heat exchanger.

Heat transfer in sinusoidal corrugated-plate channels was studied for *Re* up to $Re = 1000$ and Prandtl numbers between 5 and 150 [15]. Different amplitudes of the wall waviness, a_w, and the corrugation wave length, λ'', were studied (Figure 5.8).

In Figure 5.9 Nusselt numbers as function of the Prandtl and Reynolds numbers are reproduced for a typical wall corrugation aspect ratio of $\gamma' = 0.5$, with $\gamma' = 4 \cdot a_w / \lambda''$ (see Figure 5.8). As expected, the Nusselt number increases with increasing Reynolds number. For viscous liquids with $Pr = 150$ an increase of the heat transfer performance of roughly one order of magnitude is obtained compared to a slit channel with $H/W = > 0$.

The influence of the aspect ratio on Nusselt number is seen in Figure 5.10. In this figure, the Nusselt number is determined for a highly viscous liquid with $Pr = 150$ as function of the Reynolds number for different corrugation aspect ratios, γ'. Compared to the performance of a straight channel with slit geometry (H/S=>0) and constant wall temperature ($Nu = 7.54$), the heat transfer coefficient is enhanced several times depending on γ' and *Re.* For $\gamma' = 1$ and $Re = 100$ Nu is 34 times higher than in a slit channel. From the figures it becomes evident that a significant increase of the heat transfer performance can be obtained only at Reynolds numbers $Re \geq 100$ in the swirl flow regime.

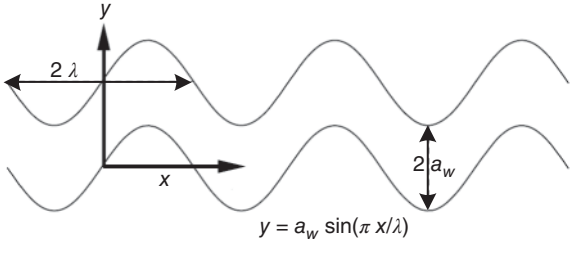

Figure 5.8 Parallel-plate channel with sinusoidal wall waviness [15]. (Adapted with permission from Elsevier.)

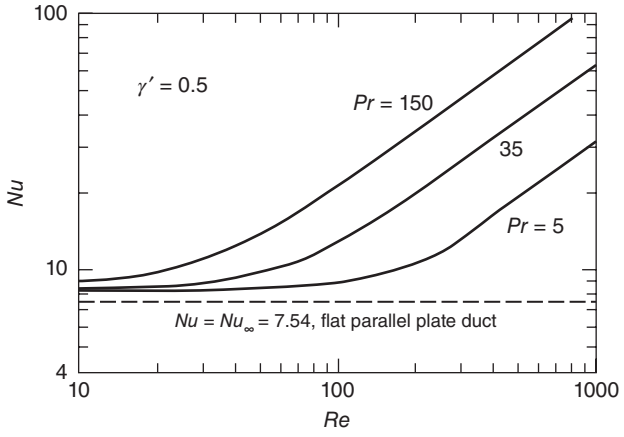

Figure 5.9 Nusselt numbers in sinusoidally corrugated channels as function of Reynolds and Prandtl number. Aspect ratio, $\gamma' = 0.5$. (Adapted with permission from Elsevier.)

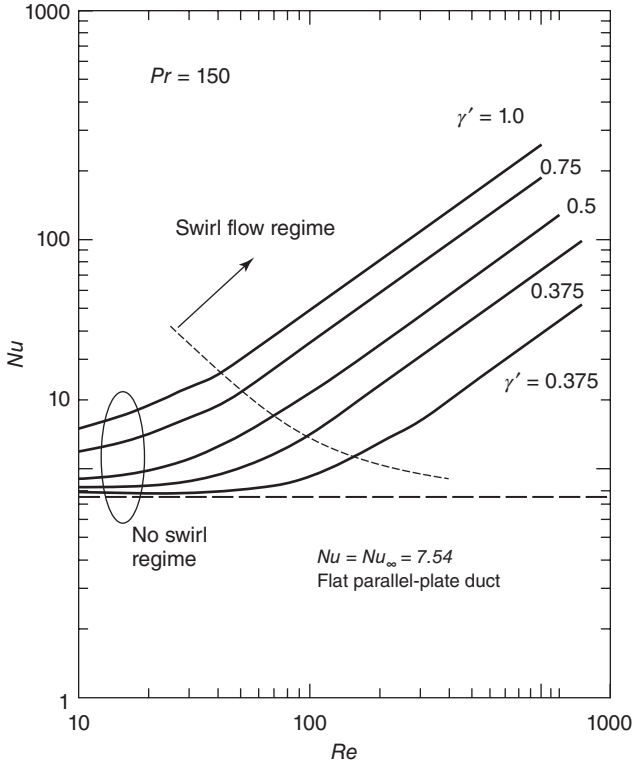

Figure 5.10 Nusselt numbers in sinusoidally corrugated channels obtained for viscous liquids as function of Re and aspect ratio [15]. (Adapted with permission from Elsevier).

5.2.3
Complex Channel Geometries

Often complex geometries are used for the design of MSR. An example is the channel structure developed by the chemical company LONZA Ltd., Switzerland [16], where mixing elements are integrated in the microchannels (Figure 5.11). In these cases, the estimation of the active heat transfer surface area and the heat transfer coefficients are hardly possible. Therefore, the introduction of an overall volumetric heat transfer coefficient (U_v) is useful.

$$\dot{Q} = U_v \cdot V_R \cdot (T_c - T) \tag{5.18}$$

where V_R is the internal reactor volume of the device.

Whereas V_R can be easily calculated from the design of the microreactor, the heat transfer coefficient must be determined experimentally by measuring the heat transferred under defined conditions in a nonreacting system.

$$U_v = \frac{\dot{Q}}{V_R \cdot (T_c - T)} \tag{5.19}$$

The overall volumetric heat transfer coefficient is correlated to the conventional heat transfer coefficient by

$$U_v = U\frac{A_{\text{ref}}}{V_R} = U \cdot a_{\text{ref}} \tag{5.20}$$

A_{ref} is a reference heat exchange area.

The global heat transfer coefficient comprises all transfer resistances as shown in Equation 5.8. In general, a minimum volumetric heat transfer coefficient of $U_v \geq 1\,\text{MW m}^{-3}\,\text{K}^{-1}$ is required for fast and exothermic reactions [16].

5.2.4
Multichannel Micro Heat Exchanger

Because of the small thermal diffusion paths and the high specific surface area, micro heat exchangers are used for rapid heat transfer between hot and cold fluids. Compared to conventional heat exchangers, the size can be considerably

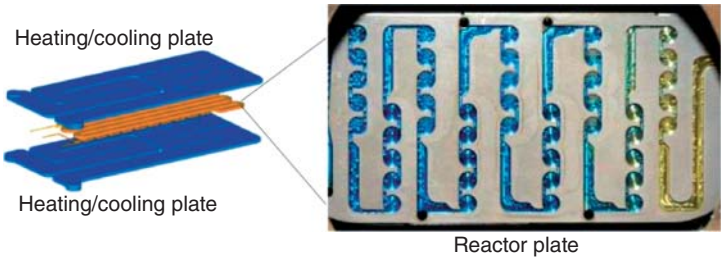

Figure 5.11 Channel structure of a microreactor plate between two heat exchanger plates [17]. (Adapted with permission from Elsevier.)

reduced. A characteristic feature of the multichannel micro heat exchanger is that the thickness of the channel walls is often comparable to the dimensions of the channel itself. This is an important difference from macroscopic devices, in which the width of the open channels is much larger than the wall thickness. In consequence, axial heat conduction in the channel walls cannot be neglected in microstructured devices. The influence of axial heat transfer is particular important for gas-to-gas heat exchanger.

The influence of the wall material on the performance of a countercurrent micro heat exchanger was studied theoretically by Stief *et al.* [18]. The authors considered nitrogen gas flow through channels of 50 µm height, 500 µm width, and 10 mm length. The thickness of the separating walls was varied between 125 and 500 µm.

If the thermal conductivity of the wall material is changed, different axial temperature profiles in the channels with hot and cold gases and within the channel walls are obtained.

If the wall heat conductivity is very low ($\lambda_{wall} = >0$) no heat is exchanged and the temperature in the channels stay constant (Figure 5.12a). At very high thermal conductivity, a constant wall temperature results and the temperatures of the gases change very rapidly in the entrance regions of the channels (Figure 5.12c). Using wall material with intermediate thermal conductivity leads to a nearly linear axial temperature profile as shown in Figure 5.12b.

The performance of the heat exchanger is characterized by its efficiency, η_{HEX}, which is the ratio of the actual heat transferred and the maximum.

In the case of equal volume flows of two identical fluids, the efficiency is given by:

$$\eta_{HEX} = \frac{T_{1,0} - T_1}{T_{1,0} - T_{2,0}} = \frac{T_{2,0} - T_2}{T_{1,0} - T_{2,0}} \tag{5.21}$$

The heat exchanger efficiency was investigated as function of the heat conductivity of the wall λ_{wall} for a countercurrent micro heat exchanger. At very low heat conductivity (λ_{wall} <0.1 W m^{-1} K^{-1}), the heat conductivity through the wall becomes the limiting factor for heat transfer. No influence of the axial heat conduction within the wall is observed, on account of the low heat conductivity. The picture

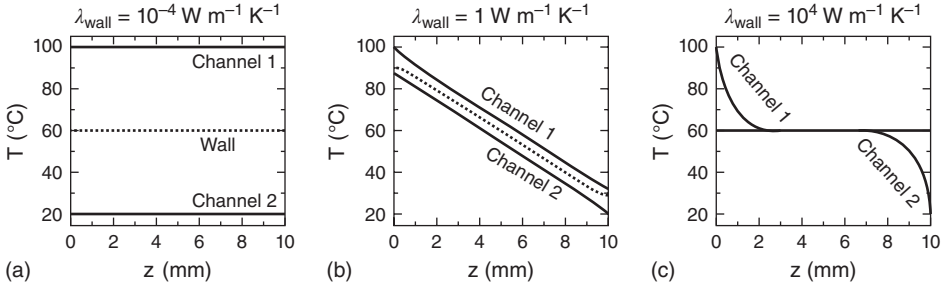

Figure 5.12 (a–c) Axial temperature profiles in microchannel gas-to-gas heat exchanger with different wall heat conductivities [18]. (Adapted with permission from Wiley.)

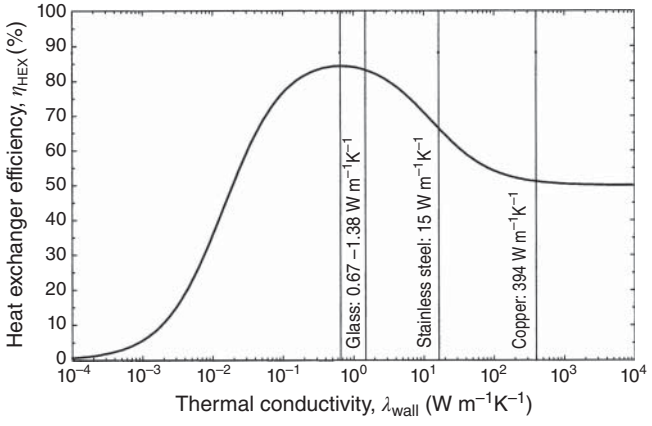

Figure 5.13 Efficiency of a gas-to-gas micro heat exchanger as a function of the heat conductivity of the wall [18]. (Adapted with permission from Wiley.)

is completely different when the heat conductivity of the wall is very high. In this case heat transfer is no longer limited by the heat conductivity of the wall and another adverse effect becomes apparent. The high axial heat conductivity of the wall leads to a leveling out of the axial temperature differences in the wall material and the device becomes indistinguishable from a cocurrent heat exchanger, which is limited to an efficiency of 50% at equal volume flows of the same fluid in both channels. At $\lambda_{wall} = 0.66\,W\,m^{-1}\,K^{-1}$, the efficiency passes through a maximum value of 84.5% as shown in Figure 5.13. Under these conditions axial conduction in the channel walls is suppressed and transversal conductivity is still sufficient for an efficient heat transfer. Therefore, for gas-to-gas micro heat exchangers, materials with low thermal conductivities like glass or polymers are preferable.

5.2.5
Microchannels with Two Phase Flow

Fluid–fluid systems are widely used for chemical transformations. Examples are halogenations, hydrogenations, and hydroformylations for gas–liquid reactions and nitrations, polymerizations, and cyclization for liquid–liquid systems. In addition, two-phase slug flow reactors can be used to get narrow residence time distribution at low liquid Reynolds numbers as demonstrated in chapter 3. Most of the reactions mentioned above are highly exothermic and heat evacuation is an important issue for efficient temperature control.

Theoretical and experimental studies demonstrated that segmented gas/liquid flow enhances the heat transfer considerably compared to a single flow. Multiphase flow simulations revealed mainly two mechanisms explaining the increase of the Nusselt number, namely the circulation within the liquid slugs and the disturbing and renewing of the fluid layer near the wall by the gas bubbles. Detailed multiphase simulations for cylindrical channels by Lakehal *et al.* [19] lead to the

following relation, allowing the estimation of the *Nu* in segmented flow:

$$Nu_{\text{seg}} \cong Nu_{\infty} + 0.022 \cdot Pr_L^{0.4} \text{Re}_{\text{LS}}^{0.8} \tag{5.22a}$$

where Nu_{∞} is the asymptotic value for fully developed single-phase flow, equal to 3.66 for constant wall temperature in cylindrical pipes, and Re_{LS} is the liquid slug Reynolds number [19, 20]:

$$Re_{\text{LS}} = \frac{u_b \cdot d_h}{\nu_L \cdot L_b/(L_b + L_{\text{slug}})} \tag{5.22b}$$

The theoretical estimations are confirmed by experimental studies carried out with a squared channel of 500 µm height and width and a length of 25 mm [20].The authors used water and air as fluids. Segmented flow with recirculating wakes could be generated for Bond numbers of $Bo = \rho \cdot g \cdot d_h^2/\sigma < 3.36$ and capillary numbers of $Ca_L = u_b \cdot \mu_L/\sigma < 0.04$ with σ, the interfacial tension. The experimental results confirm the general trends predicted with Equation 5.22. The measured Nusselt numbers are slightly lower than the predicted ones for Reynold numbers $Re_{\text{LS}} < 400$. This may be explained by the fact that the asymptotic Nusselt number in square shaped channels is with $Nu_{\infty} = 2.98$ lower compared to circular pipes with $Nu_{\infty} = 3.66$ (see Table 5.1).

The increase of heat transfer performance of segmented flow in microchannels compared to single-phase flow was also found for liquid–liquid systems [21]. The experimental studies were carried out with square shaped channels of 100 µm width and height. Segmented flow was generated in the microchannel with water as continuous and mineral oil as dispersed phase. The oil:water ratio was varied between 10:100 and 30:100. Experimental results are summarized in Figure 5.14.

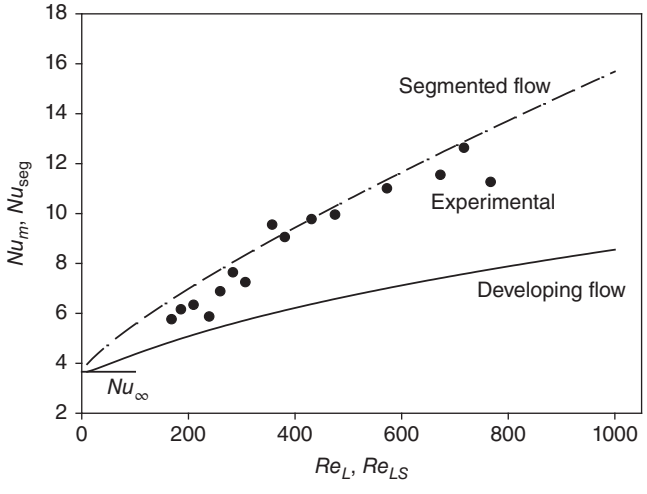

Figure 5.14 Estimated Nusselt numbers for segmented flow [19] and hydrodynamically developing single-phase flow in cylindrical pipes ($Pr_L = 7$; $d_h/L_t = 0.02$) [20]. (Experimental values taken from Ref. [20]) (squared channel, $Pr_L = 7$; $d_h/L_t = 0.02$).

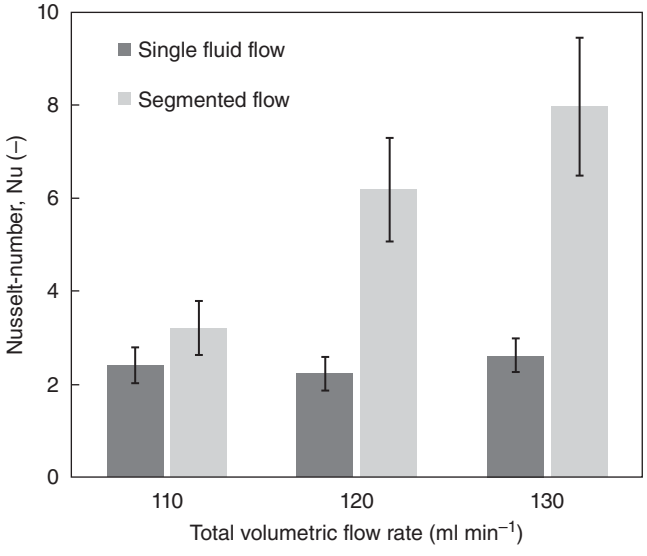

Figure 5.15 Nusselt number at various flow rates. Comparison between segmented and single-phase flow in squared microchannels [21]. (Adapted with permission from Elsevier.)

The figure confirms the significant Nusselt number enhancement for segmented flow in microchannels. Up to fourfold increase was observed for a total throughput of 130 µl min^{-1}, corresponding to a linear velocity of 0.217 m s^{-1} (Figure 5.15).

5.3
Temperature Control in Chemical Microstructured Reactors

On the basis of a detailed analysis [22], chemical reactions can be classified in different categories depending on their kinetics. Following this classification, three types of reactions are identified:

- Type A reactions are very fast with characteristic reaction times of $t_r < 1$ s. Such reactions are mostly influenced or even completely controlled by the mixing process. In consequence, the reaction and the accompanied heat production take place near the entrance in the mixing zone.
- Type B reactions are fast with characteristic times between 1 s and 10 min. They are mainly kinetically controlled. Temperature control may become critical for systems with high reaction enthalpy.
- Type C reactions are considered as slow ($t_r > 10$ min). They are normally carried out in batch-wise operated vessels. Nevertheless, microstructured devices may be advantageous, if safety or product quality is an important issue.

Generally, reactions of type A are considered as instantaneous and the transformation rate is limited by mixing. In this case, the intensity of mixing controls the heat production.

Heat evacuation for the reaction of type A can be critical even if the volumetric heat transfer coefficient U_v is high. The heat production is maximum in the mixing zone resulting in hot spot formation because of limited cooling even for a typical microchannel size (500 µm). Four strategies can be applied in order to reduce the height of the hot spots without dilution of the reactants [23]:

- Reduction of channel diameter: it increases the specific interfacial area a, which is inversely proportional to the reactor diameter d_h. However, further reduction in reactor size increases the risk of clogging and results in higher specific energy consumption because of higher pressure drop to overcome during pumping.
- Active heat exchange or mixing elements like fins or static mixers [24]: this would increase the overall heat exchange coefficient. However, the gained benefits should not increase the technical complexity.
- Use of highly heat conducting material for microreactors: it distributes the locally produced heat along the length of the microreactor.
- Multi-injection concept: spread heat production along the channel length to reduce local heat production and thus diminishing hot spot.

The amount of heat produced during a reaction per unit of reactor volume, that is, specific heat production ($\dot{q}_r$), is the product of the effective reaction rate and reaction enthalpy:

$$\dot{q}_r = r_{j,\text{eff}} \cdot (-\Delta H_{r,j}) \tag{5.23}$$

with $r_{j,\,\text{eff}}$ the effective reaction rate. For instantaneous reactions (type A), the effective reaction rate is controlled by the mixing process characterized by the mixing time, t_{mx}. The effective transformation can be represented by the initial concentration and the inverse of the mixing time as given in the following equation (Example 5.2):

$$\dot{q}_r = r_{j,\text{eff}} \cdot (-\Delta H_{r,j}) = \frac{1}{t_{\text{mx}}} c_0 \cdot (-\Delta H_{r,j}) \tag{5.24}$$

The heat evacuated by maintaining constant wall temperature is directly proportional to the temperature difference between reactor and constant cooling temperature (T_c) as

$$\dot{q}_{\text{ex}} = U_v \cdot (T - T_c) \tag{5.25}$$

Example 5.2: Heat evacuation for a an instantaneous reaction.

A quasi-instantaneous and exothermic reaction ($-\Delta H_r = 120\,000\ \text{kJ kmol}^{-1}$ of limiting reactant) is carried out in a microchannel with circular cross section. The mixing time is $t_{\text{mx}} = 0.5\ \text{s}$. Estimate the tube diameter required to evacuate the heat, if the heat transfer is limited by the heat transfer in the reaction channel ($U_v \cong h_r \cdot a = h_r \cdot 4/d_h$) and the temperature difference between reaction mixture and cooling fluid is 10 K. The initial concentration of limiting

reactant is $c_{1,0} = 0.9\,\mathrm{kmol\,m^{-3}}$. We consider the asymptotic Nusselt number for fully developed laminar flow. The thermal conductivity of the reaction mixture is $1.4 \cdot 10^{-4}\,\mathrm{kW\,m^{-1}\,K^{-1}}$.

Solution:

The amount of heat evacuated during the reaction is

$$\dot{q}_r = \frac{c_0}{t_{\mathrm{mx}}} \cdot (-\Delta H_r) = \frac{0.9}{0.5} \cdot 120\,000 = 2.16 \cdot 10^5\,\mathrm{kW\,m^{-3}}$$

With $Nu_\infty = 3.66$ for circular channels we obtain (Equation 5.9):

$$\dot{q}_r = \dot{q}_{\mathrm{ex}} = h \cdot a \cdot (T - T_c); h = \frac{Nu_\infty \lambda_f}{d_h}; \frac{a = 4}{d_t}$$

$$d_t = \sqrt{\frac{Nu_\infty \lambda_f}{\dot{q}_r} 4 \cdot 10} = \sqrt{\frac{3.66 \cdot 1.4 \cdot 10^{-4}}{2.16 \cdot 10^5} \cdot 4 \cdot 10} = 3.08 \cdot 10^{-4}\,\mathrm{m} = 308\,\mu\mathrm{m}$$

Thus, a microchannel reactor with 308 µm diameter would be required to evacuate the heat.

In Example 5.2, the calculated diameter of the reaction channel was estimated for the maximum heat produced at the mixing point at the reactor entrance. As a first order process is assumed for the mixing process, the reactant concentration will diminish with increasing residence time, and, respectively, with increasing distance from the reactor entrance. In consequence, transformation rate as well as heat production will decrease. This in turn will lead to an axial temperature profile with the maximum temperature at the entrance. This maximum temperature corresponds to the inlet temperature ($T_{\mathrm{max}} = T_0$). For a more correct design of the reactor the local heat and mass balances must be considered.

5.3.1
Axial Temperature Profiles in Microchannel Reactors

Because of the small diameter of microchannels ($d_h < 1\,\mathrm{mm}$), a homogeneous temperature in radial direction can be assumed. In the gas phase, mass and heat transport have the same characteristic time. Exceptions are fast gas phase reactions with high activation energies such as combustions where radial temperature gradients exist.

For the following discussion we consider ideal plug flow behavior of the microchannel reactor. The material balance for a small volume element (ΔV)

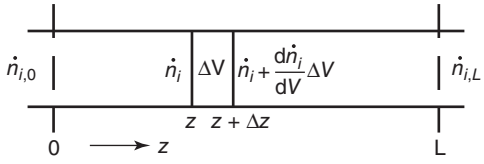

Figure 5.16 Mass balance in a stationary ideal plug flow reactor.

shown in Figure 5.16 at steady state is written as

$$-\frac{\mathrm{d}\dot{n}_i}{\mathrm{d}V} + R_i = 0 \tag{5.26}$$

Assuming the cross sectional area to be constant, $\mathrm{d}V = A_{\mathrm{cs}} \cdot dz$, the above equation can be written as

$$\frac{\mathrm{d}n_i}{\mathrm{d}z} = A_{\mathrm{cs}} \cdot R_i \tag{5.27}$$

A_{cs} is the cross sectional area of the channel.

The reactor volume is obtained by integration:

$$V = V_R = \int_{\dot{n}_{i,0}}^{\dot{n}_{i,L}} \frac{\mathrm{d}\dot{n}_i}{R_i} \tag{5.28}$$

Introducing the conversion, *X,* for the key reactant A_1 as

$$X = \frac{\dot{n}_{1,0} - \dot{n}_{1,L}}{\dot{n}_{1,0}} \tag{5.29}$$

Equation 5.28, becomes

$$V = V_R = \int_0^{X_L} \frac{\mathrm{d}X}{-R_i} = \dot{V}_0 c_{1,0} \int_0^{X_L} \frac{\mathrm{d}X}{-R_i} \tag{5.30}$$

To simplify the energy balance, the work done on the reacting fluid is neglected and constant heat capacity and reaction enthalpy is assumed. The steady state temperature profile of the fluid without the influence of axial conductivity can be calculated by considering the energy balance (Equation 5.31) simultaneously with the material balance (Equation 5.32).

$$\frac{\mathrm{d}T}{\mathrm{d}V} = \frac{\mathrm{d}T}{A_{\mathrm{cs}} \cdot \mathrm{d}z} = \underbrace{\frac{(-R_1) \cdot (-\Delta H_r)}{\dot{m} \cdot \bar{c}_p}}_{\substack{\text{Heat produced} \\ \text{due to the reaction}}} - \underbrace{\frac{U \cdot a \cdot (T - T_c)}{\dot{m} \cdot \bar{c}_p}}_{\substack{\text{Heat removed by maintaining} \\ \text{constant cooling temperature}}} \tag{5.31}$$

$$\frac{\mathrm{d}X}{\mathrm{d}V} = \frac{\mathrm{d}X}{A_{\mathrm{cs}} \cdot \mathrm{d}z} = \frac{-R_1}{\dot{n}_{1,0}} = \frac{-R_1}{\dot{V}_0 \cdot c_{1,0}} \tag{5.32}$$

In this equation, $\dot{m}$ represents the mass flow rate, $\bar{c}_p$ is the mean specific heat capacity of the mixture in the considered temperature range, and U is the global heat transfer coefficient.

The overall heat transfer coefficient consists of different contributions from heat transfer resistances, R_{th}. For simplicity, we do not consider different exchange areas of the various heat transfer resistances. The heat transfer coefficient in the reaction channel h_r is correlated with the Nusselt number, while the thermal resistances in the wall and the cooling channel are lumped together and replaced with a coefficient C_{Rth} [17].

$$\frac{1}{U} = \frac{1}{h_r} + R_{th} = \frac{d_h}{Nu \cdot \lambda_f} + R_{th} \Rightarrow U = C_{Rth} \cdot h_r = C_{Rth} \frac{Nu \cdot \lambda_f}{d_h} \tag{5.33}$$

C_{Rth} is the ratio between the overall heat transfer coefficient and the heat transfer coefficient in the reactor channel: $C_{Rth} = U/h_r \leq 1$

If the transfer resistances in the reactor wall and the cooling channel are similar $1/h_r \cong R_{th}$ a coefficient of $C_{Rth} = 0.5$ results. Typical values for C_{Rth} are 0.1–0.5 in liquid phase microreactors, depending on wall material and the thermal fluid used. For gas phase reactions the main resistance for heat transfer is mostly on the reaction side, if a liquid is used as cooling fluid ($C_{Rth} = >1$).

If heat transfer is referred to the exchange area of the reactor channel, the specific heat exchange surface a is given by $a = A_{ex}/V_R$. For channels surrounded by the cooling medium, that is, in a shell and tube heat exchanger reactor, the specific surface area corresponds to $a = A_{ex}/V_R = 4/d_h$.

Assuming constant cross section, Equation 5.31 can be written as

$$\frac{dT}{dZ} = \Delta T_{ad} \frac{(-R_1) \cdot \tau_{PFR}}{c_{1,0}} - \frac{\cdot U \cdot \tau_{PFR} \cdot}{\rho_0 \cdot \bar{c}_p} \frac{4}{d_h} (T - T_c)$$
$$\text{with } Z = V/V_R; \tau_{PFR} = V_R/\dot{V}_0; \tag{5.34}$$

ΔT_{ad} the adiabatic temperature rise:

$$\Delta T_{ad} = \frac{c_{1,0} \cdot (-\Delta H_r)}{\rho_0 \cdot \bar{c}_p} \tag{5.35}$$

with $c_{1,0}$ as the inlet concentration of the limiting reactant. From Equation 5.32 it follows:

$$\frac{dX}{dZ} = \frac{-R_1 \cdot \tau_R}{c_{1,0}} \tag{5.36}$$

To determine the axial temperature profile in the tubular reactor, Equations 5.34 and 5.36 must be solved simultaneously by numerical integration. The design of microchannel reactors is discussed in detail in Example 5.3 and 5.4

Example 5.3: Overall heat evacuation for a type B reaction.

The microchannel reactor described in Example 5.1 is previewed for a type B reaction with a characteristic reaction time of $t_r = 5$ s at 323 K. The reaction is irreversible and of first order. The reaction enthalpy

is $\Delta H_r = -150\ 000\,\mathrm{kJ\,kmol^{-1}}$ and the activation energy is found to be $E_a = 80\,\mathrm{kJ\,kmol^{-1}}$. The reaction will be carried out at 323 K in toluene as solvent and a residence time of $\tau_{\mathrm{PFR}} = 15\,\mathrm{s}$. The inlet concentration is fixed to $c_{1,0} = 0.7\,\mathrm{kmol\,m^{-3}}$. The temperature of the cooling fluid is 10 K below the reaction temperature at the reactor inlet to evacuate the reaction heat. Estimate the reactor performance and the axial temperature profile.

Solution:

The maximum total heat produced ($X = 1$) is given by

$$\dot{q}_r = \frac{c_{1,0} \cdot (-\Delta H_r)}{\tau_{\mathrm{PFR}}} = \frac{0.7 \cdot 150\,000}{15} = 7 \cdot 10^3\,\mathrm{kW\,m^{-3}}$$

With a volumetric global heat transfer coefficient of $U_v = 1.06 \cdot 10^3\,\mathrm{kW\,m^{-3}\,K^{-1}}$ and a temperature difference of $\Delta T = 10\,\mathrm{K}$, the maximum total heat generated can be evacuated.

$$\dot{q}_{\mathrm{ex}} = U_v \cdot \Delta T = 10.6 \cdot 10^3\,\mathrm{kW\,m^{-3}}$$

The adiabatic temperature rise can be calculated as:

$$\Delta T_{\mathrm{ad}} = \frac{c_{1,0} \cdot (-\Delta H_r)}{\rho_0 \cdot \bar{c}_p} = \frac{0.7 \cdot 150\ 000}{867 \cdot 1.72} = 70.4\,\mathrm{K}$$

In Figure 5.17 the reactor temperature and the conversion as function of the distance from the reactor entrance is shown. In spite of the low cooling temperature, the temperature increases within the first 20% of the reactor length. The maximum temperature is roughly 20 K higher than the inlet temperature. The steep temperature increase is accompanied with a drastic increase of the conversion from X = 0 to X = 0.8. The diminished reactant concentration leads to low transformation rates and low heat production, and the reactor temperature decreases and attains nearly the temperature of the cooling fluid at the reactor outlet. It is important to note that measuring the outlet temperature gives no indication of the reaction control within the reactor. The conversion finally reaches 0.973 at the reactor outlet. The specific reactor performance reaches $L_{p,v} = 45.41\,\mathrm{mol\,m^{-3}\,s^{-1}}$.

The influence of the inlet temperature on the axial temperature profile in the microchannel reactor is illustrated in Figure 5.18. All other reaction conditions are kept constant. The initial temperature difference between the cooling fluid and the reaction mixture at the inlet is in all cases identical ($T_0 - T_c = 10\,\mathrm{K}$). At the reactor outlet the temperature reaches nearly the cooling temperature for all inlet conditions. But, the maximum temperature increases drastically with an increase of T_0. The important increase of the maximum temperature because of a small change of the inlet conditions is called *parametric sensitivity* and can be observed for fast and exothermic reactions in tubular reactor. In the domain of high parametric sensitivity the reactor is difficult to control and important temperature excursions cannot be avoided. High local temperatures may lead to important

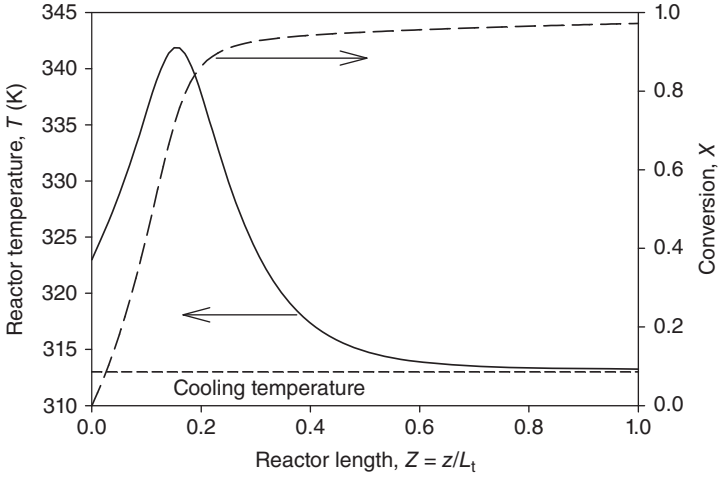

Figure 5.17 Axial temperature and conversion profile (Example 5.3).

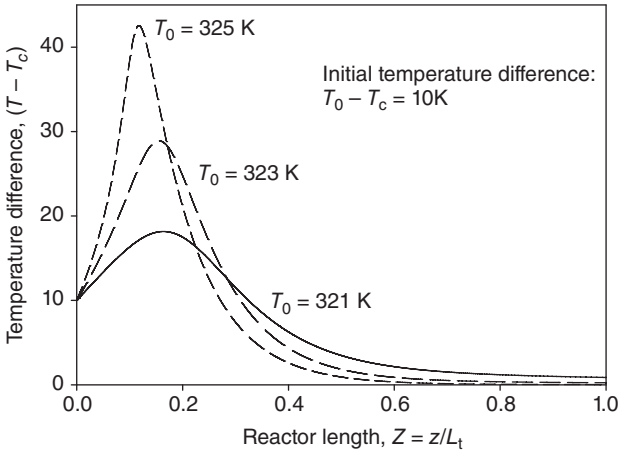

Figure 5.18 Influence of the inlet temperature on the axial temperature profile. (Data taken from Example 5.3.)

losses of product selectivity and quality, or may even damage the used catalyst or reactor. Therefore, high parametric sensitivity of chemical reactors must be avoided.

5.3.2 Parametric Sensitivity

For given reaction kinetics the thermal behavior of tubular reactors depends on three different parameters:

The Arrhenius number:

$$\gamma = \frac{E}{R \cdot T_c} \tag{5.37}$$

The heat production potential:

$$S' = \frac{(-\Delta H_r) \cdot c_0}{\rho \cdot c_p \cdot T_c} \cdot \gamma = \frac{\Delta T_{\mathrm{ad}}}{T_c} \cdot \gamma = \Delta T_{\mathrm{ad}} \frac{E}{R \cdot T_c^2} \tag{5.38}$$

and the ratio of the characteristic reaction time to the cooling time:

$$N' = \frac{t_r}{t_c}$$
$$t_r = \frac{1}{k(T_c) \cdot c_{1,0}^{n-1}}; t_c = \frac{\rho \cdot c_p}{U_v} \tag{5.39}$$

The characteristic reaction time is calculated with the temperature of the cooling medium (T_c) respectively the inlet temperature (T_0). In the following discussion the inlet and the cooling temperature are supposed to be identical ($T_0 = T_c$).

To facilitate the discussion on the influence of the above-defined parameters (Equations 5.37–5.39) on the reactor behavior and the parametric sensitivity, Equations 5.34 and 5.36 are given in a dimensionless form. According to the studies of Barkelew [25] the mean residence time is referred to the characteristic reaction time and the temperature is given in the form of a relative temperature difference normalized with the Arrhenius number (Equation 5.41).

$$\tau_R' = \frac{\tau}{t_r} = \tau \cdot k_0 \ \exp\left(\frac{-E}{R \cdot T_c}\right) \cdot c_{1,0}^{n-1} \tag{5.40}$$

The dimensionless residence time, τ_R', can be interpreted as a first Damköhler number, defined with the characteristic reaction time calculated with the temperature of the cooling medium.

$$\Delta T' = \frac{(T - T_c)}{T_c} \cdot \gamma = \frac{(T - T_c)}{T_c^2} \frac{E}{R} \tag{5.41}$$

With these definitions the conversion and the temperature as function of the dimensionless channel length can be calculated.

$$\frac{\mathrm{d}X}{\mathrm{d}Z} = \tau_R' \cdot \exp\left(\frac{\Delta T'}{1 + \Delta T'/\gamma}\right) \cdot (1 - X)^n \cong \exp(\Delta T') \cdot (1 - X)^n \tag{5.42}$$

$$\frac{\mathrm{d}\Delta T'}{\mathrm{d}Z} = \tau_R' \cdot S' \cdot \exp\left(\frac{\Delta T'}{1 + \Delta T'/\gamma}\right) \cdot (1 - X)^n - \tau_R' \cdot N' \cdot \Delta T'$$
$$\cong \tau_R' \cdot S' \cdot \exp(\Delta T') \cdot (1 - X)^n - \tau_R' \cdot N' \cdot \Delta T' \tag{5.43}$$

where N' is the ratio of characteristic reaction time (t_r) to cooling time (t_c) and S' is the heat production potential as defined in Equations 5.39 and 5.38.

The Arrhenius numbers are in general high, $\gamma > 20$. Therefore, the term $\Delta T'/\gamma$ is small and can mostly be neglected and Equations 5.42 and 5.43 are often given in a simplified form:

$$\frac{dX}{dZ} \cong \exp(\Delta T') \cdot (1 - X)^n \tag{5.44}$$

$$\frac{d\Delta T'}{dZ} \cong \tau'_R \cdot S' \cdot \exp(\Delta T') \cdot (1 - X)^n - \tau'_R \cdot N' \cdot \Delta T' \tag{5.45}$$

The temperature change along the dimensionless reactor length, Z, is a result of the difference between the heat produced and removed (Figure 5.19a). In the first part of the channel, the heat produced by reaction exceeds the heat evacuated through the channel wall. As a consequence, the reaction mass is heated up to a maximum. At temperature maximum, commonly called "*hot spot*," the produced heat by reaction is entirely removed by the cooling system $\tau'_R \cdot S' \cdot \exp(\Delta T') \cdot (1 - X)^n = \tau'_R \cdot N' \cdot \Delta T'$. As the main amount of the reactant is transformed within the region of the temperature peak (Figure 5.19b) the concentration drops down and the reaction rate diminishes. In the second part of the channel, heat production is low compared to the heat transfer performance and the reaction mass is cooled down close to the cooling temperature, T_c.

It is important to note that decreasing the cooling intensity from $N' = 45$ to 30 and further to $N' = 25$ has a moderate influence on the hot spot formation. The situation changes drastically for values of $N' < 25$. In this range, even small variations of the cooling intensity leads to tremendous variations of the maximum temperature. The reactor is operated in a region of high parametric sensitivity.

The reactor behavior of a second order reaction shown in Figure 5.20 corresponds to the behavior of a first order reaction (Figure 5.19). But, the region of

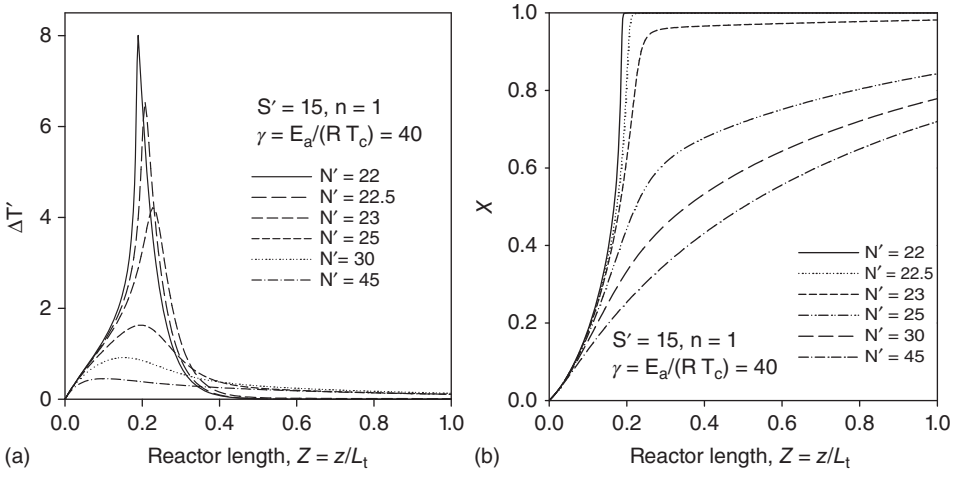

Figure 5.19 Axial temperature (a) and conversion profile (b) in a cooled microchannel for different cooling intensity, N' ($n = 1$, $T_0 = T_c$).

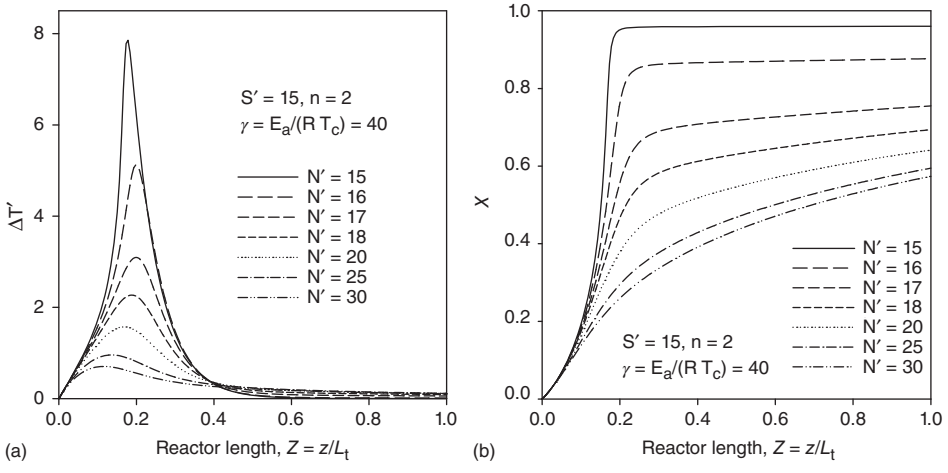

Figure 5.20 Axial temperature (a) and conversion profile (b) in a cooled microchannel for different cooling intensity, N' ($n = 2$, $T_0 = T_c$).

high parametric sensitivity is shifted to lower values of N' for the same heat production potential ($S' = 15$).

The dimensionless reactor length, Z, can be eliminated by dividing Equation 5.45 by Equation 5.44 to get the reaction temperature as function of the conversion.

$$\frac{\mathrm{d}\Delta T'}{\mathrm{d}X} = S' - N' \cdot \Delta T' \cdot \exp\left(\frac{-\Delta T'}{1 + \Delta T'/\gamma}\right) \frac{1}{(1-X)^n} \cong S' - N' \cdot \Delta T' \frac{\exp(-\Delta T')}{(1-X)^n} \tag{5.46}$$

For the temperature maximum follows: $\frac{\mathrm{d}\Delta T'}{\mathrm{d}X} = 0$. This allows estimating the conversion at the hot spot neglecting $\Delta T'/\gamma$ compared to 1 in the denominator of the exponential function.

$$\begin{aligned} \frac{\mathrm{d}\Delta T'}{\mathrm{d}X} &= S' - N' \cdot \Delta T'_{\max} \frac{\exp(-\Delta T'_{\max})}{(1-X_{\max})^n} = 0 \\ (1-X_{\max})^n &= \frac{N'}{S'} \cdot \Delta T'_{\max} \exp(-\Delta T'_{\max}) \\ X_{\max} &= 1 - \left[\frac{N'}{S'} \cdot \Delta T'_{\max} \exp\left(-\Delta T'_{\max}\right)\right]^{\frac{1}{n}} \end{aligned} \tag{5.47}$$

The ratio between N' and S' is an important parameter for the general discussion of the stability and parametric sensitivity of chemical reactors. N'/S' corresponds to the reciprocal Semenov number [26]

$$\frac{N'}{S'} = \frac{1}{Se} = \frac{U_v}{\rho \cdot c_p} \frac{1}{k(T_c) c_{1,o}^{n-1}} \frac{RT_c^2}{\Delta T_{\mathrm{ad}} E_a} = \frac{U_v}{(-\Delta H_r) k(T_c) c_{1,o}^{n}} \frac{RT_c^2}{E_a} \tag{5.48}$$

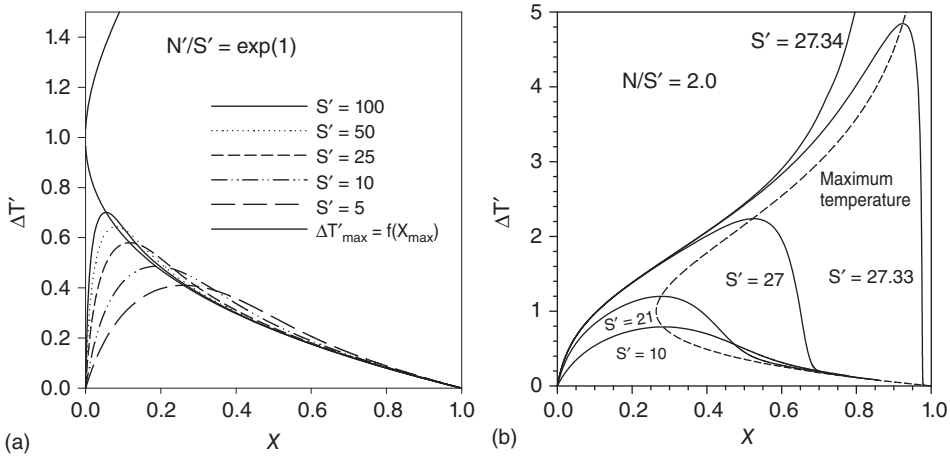

Figure 5.21 Temperature profile and maximum temperature in tubular reactors. First order reaction (Adapted from Ref. [28], Figure 7.33. Copyright © 2013, Wiley-VCH GmbH & Co. KGaA.)

N'/S' can be interpreted as the ratio between the time to maximum rate, $t_{\mathrm{mr,}}$ under adiabatic conditions supposing zero order and the characteristic cooling time, t_c [27].

In Figure 5.21a the temperature as function of the conversion and the predicted maximum temperature (Equation 5.47) are shown for the parameter $N'/S' = \exp(1)$. It follows from this figure that the maximum dimensionless temperature difference cannot exceed the value of $\Delta T' = 1$, as long as the temperature difference at the reactor inlet is smaller than 1 ($\Delta T' < 1$). With the definition of the dimensionless temperature difference (Equation 5.41), we can estimate the maximum difference between the cooling temperature and the temperature of the reaction mass: $T - T_c = T_c^2 \cdot R/E$. It is evident from Figure 5.21a that no parametric sensitive region will be reached. The reactor is stable for all values of the heat production potential, S', and reaction orders $n \geq 0$ as long as $N'/S' \geq \exp(1)$.

The situation changes for $N'/S' < \exp(1)$. In Figure 5.21b the temperature profile for $N'/S' = 2$ and different values for the heat production potential, S', is shown. Starting with low values, S' is increased by increasing the inlet reactant concentration and in consequence the adiabatic temperature rise or by increasing the cooling temperature. For the supposed kinetics of an irreversible first order reaction, the maximum temperature in the reactor first increases slowly with S', but reaches a region of very high parametric sensitivity for $S' > 27$. A similar behavior can be observed for all reactions with positive reaction order ($n > 0$).

Different criteria are proposed for estimating the region of high parametric sensitivity based on accessible criteria [27]. Most of the corresponding publications are restricted to first order reactions. The published results are slightly different

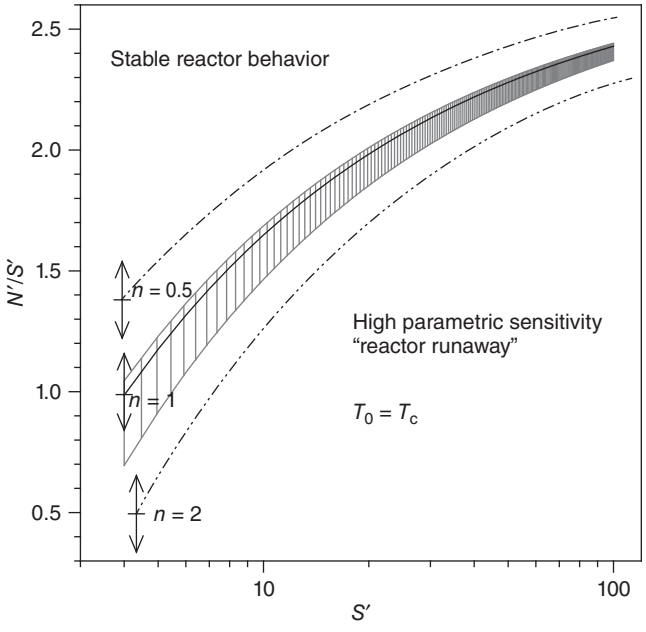

Figure 5.22 Parametric sensitivity of plug flow reactor for reactions of $n = 0.5$, 1.0, and 2.0. Area under the corresponding curves indicate high parametric sensitivity. (Adapted from Ref. [28], Figure 7.34. Copyright © 2013, Wiley-VCH GmbH & Co. KGaA.)

and are reproduced as a hatched band in Figure 5.22 separating the regions of high and low parametric sensitivity.

A very simple criterion for estimating the region of stable reactor behavior is based on a maximum temperature peak. If the maximum temperature difference is fixed to $\Delta T' = 1.2$, the following correlation is obtained for separating the region of stable operation from that of high parametric sensitivity (see Figure 5.22):

$$\frac{N'}{S'} \geq \exp(1) - \frac{B}{\sqrt{S'}} = 2.72 - \frac{B}{\sqrt{S'}} \tag{5.49}$$

The coefficient B depends on the reaction order:

$$n = 0 : B = 0$$
$$n = 0.5 : B = 2.60$$
$$n = 1 : B = 3.37$$
$$m = 2 : B = 4.57$$

The parameter N' contains the overall heat transfer coefficient, while the heat production potential is dependent on the adiabatic temperature rise, the (apparent) activation energy, and the cooling temperature. With Equation 5.49 a minimum value for N' can be estimated to assure stable reactor operation. The application of the relations presented above for the design of MSR is illustrated in Example 5.4 and 5.5.

Example 5.4: Reaction conditions for the synthesis of an ionic liquid in a slit-like MSR.

The ionic liquid, 1-ethyle-3-methyle imidazolium ethyl sulfate, is synthesized by alkylation of methyllimidazole as follows [29]

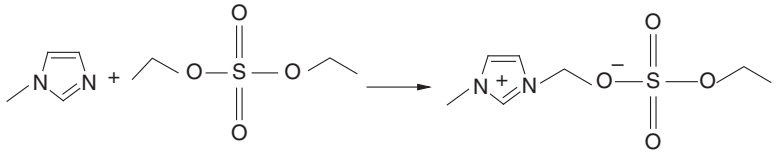

A1 **A2** **A3**

The reaction is highly exothermic and is carried out without any solvents. The reaction kinetics is fast with characteristic reaction times between several minutes to several seconds depending on the reaction temperature. The heat management is of major concern to attain high quality product and to avoid thermal runaway [30]. Preliminary studies show that reaction temperatures higher than 100 °C lead to coloration of the reaction mixture because of degradation reactions. Therefore, the hot spot temperature must be kept lower.

The microstructured slit reactor as presented in Example 5.1 is used for the solvent free synthesis of the ionic liquid.

Estimate (1) the adiabatic temperature rise, (2) the maximum cooling/inlet temperature with $T_c = T_0$, (3) the maximum temperature in the reactor, and (4) the temperature and conversion profiles along the reactor length. The relevant reaction and reactor data are summarized in Table 5.4. Suppose established temperature and laminar velocity profile.

Table 5.4 Physical properties and reaction conditions.

Reaction rate constant at $T = 313$ K	$k_{313} = 1.5 \cdot 10^{-3}$ m^3 kmol^{-1} s^{-1} [29]
Activation energy	$E_a = 86\,000$ J mol^{-1} [29]
Reaction enthalpy	$\Delta H_r = -102\,000$ kJ kmol^{-1} [29]
Density	$\rho = 1254 - 0.598 \cdot$(T/K-273) (kg m^{-3}) [31]
Viscosity	$\mu = 10.81 \cdot 10^{-4} \cdot \exp(3.38 \cdot 10^3/T)$ (mPa s) [31]
Specific heat capacity	$c_p = (5.827 \cdot 10^2 - 6.161 \cdot 10^4/T)/236.3$ (kJ kg^{-1} K^{-1}) [32]
Heat conductivity (293 K $\leq T \leq$ 353 K)	$\lambda_f = 0.18\ \ 10^{-3}$ kW m^{-1} K^{-1} [33]
Inlet concentrations	$c_{1,0} = c_{2,0} = 4.7$ kmol m^{-3}
Overall volumetric heat transfer coefficient	$U_v = 1.066 \cdot 10^3$ kW m^{-2} K^{-1} (Example 5.1)
Required conversion	$X \geq 0.75$

Solution:

1) The adiabatic temperature rise is calculated using Equation 5.35 as

$$\Delta T_{ad} = \frac{c_{1,0} \cdot (-\Delta H_r)}{\rho_0 \cdot \bar{c}_p} = \frac{4.7 \cdot 102,000}{1230 \cdot 1.63} = 239\,\text{K} \quad (T = 313\,\text{K})$$

2) Stable reactor operation can be supposed, if the following conditions are fulfilled (see Equation 5.49):

$$N' = 2.72 \cdot S' - B\sqrt{S'} \tag{5.50}$$

For second order reactions the coefficient B is found to be $B = 4.57$. Both N' and S' depend on temperature.

$$\frac{U_v}{\rho_0 c_p} \cdot \underbrace{\frac{1}{k_{313} \exp\left(-\frac{E_a}{R}\left(\frac{1}{T_c} - \frac{1}{313}\right)\right) c_{1,0}}}_{N'} = \underbrace{2.72\,\Delta T_{\mathrm{ad}} \frac{E_a}{RT_c^2} - 4.57\sqrt{\Delta T_{\mathrm{ad}} \frac{E_a}{RT_c^2}}}_{\mathrm{RHS}} \tag{5.51}$$

The maximum cooling temperature for stable operation can easily be found by plotting N' and the right-hand side (RHS) of Equation 5.51 as function of T_c. The result is shown in Figure 5.23. Obviously, a maximum temperature of $T_c = T_0 = 318\,\mathrm{K}$ is allowed for stable operation.

3) The characteristic reaction time can easily be calculated with the Arrhenius law:

$$t_{r,319} = \frac{1}{k_{313} \exp\left(-\frac{E_a}{R}\left(\frac{1}{318} - \frac{1}{313}\right)\right) \cdot c_{1,0}} = 84\,\mathrm{s}$$

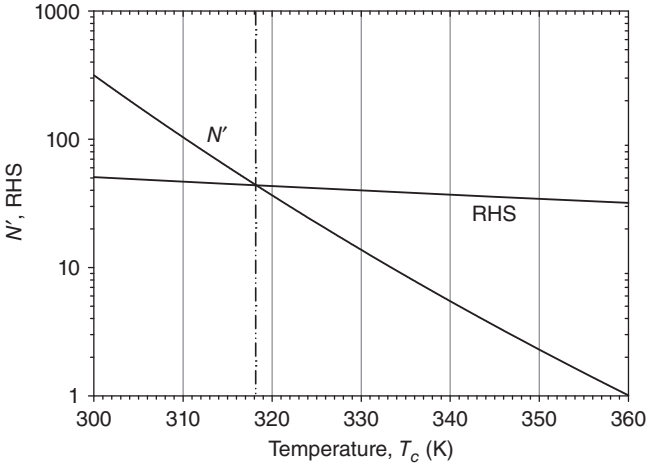

Figure 5.23 Graphical solution of Equation 5.51.

A minimum conversion of $X = 0.75$ is required. For a second order reaction the conversion in an ideal plug flow reactor depends on the first Damköhler number, *DaI,* as shown in Equation 5.52 (see Chapter 2):

$$X = \frac{DaI}{1 + DaI}; \text{with } DaI = \frac{\tau_R}{t_t} = k \cdot c_{1,0} \cdot \tau_R \tag{5.52}$$

With a characteristic reaction time of $t_r = 84$ s we need for the required conversion a residence time of $\tau_R = 252$ s.

The maximum temperature in the reactor can be estimated with the definition of the dimensionless temperature (Equation 5.41), knowing that $\Delta T'_{\max} = 1.2$. With the kinetic data summarized in Table 5.4 we obtain:

$$\Delta T'_{\max} = \frac{(T_{\max} - T_c)}{T_c^2} \frac{E_a}{R} \Rightarrow T_{\max} \cong T_c + T_c^2 \frac{R}{E_a} \cong 328\,\text{K}$$

4) The simulated axial temperature and conversion is calculated by numerical integration of Equations 5.34 and 5.36 with the data of Table 5.4. The results are reproduced in Figure 5.24.

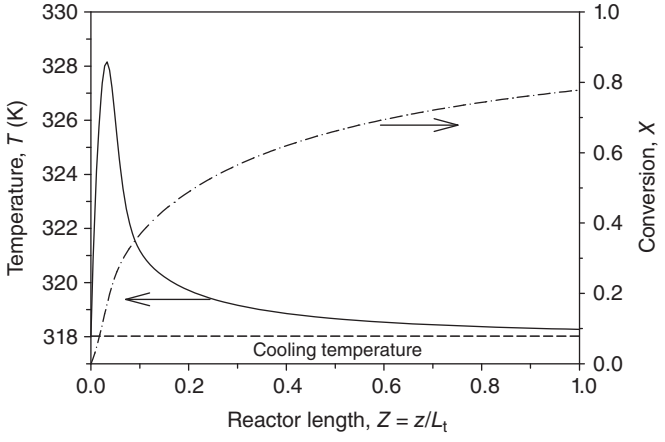

Figure 5.24 Axial temperature and conversion profile (Example 5.4).

The simulation results confirm the estimated maximum temperature allowing safe reactor operation. The conversion is slightly higher ($X = 0.78$) than predicted on the basis of an isothermal reactor operation at 318 K. This is because of the temperature peak near the reactor entrance. To complete the reaction a second reactor operating at higher temperature is needed. As the inlet concentration of the second reactor is relatively low ($c_{1,0} \cong 1\,\text{kmol m}^{-3}$) temperature control is facilitated.

Example 5.5: Design of a multichannel MSR for the high performance production of an ionic liquid.

It is planned to use a multichannel microreactor for the synthesis of the ionic liquid, 1-ethyle-3-methyle imidazolium ethyl sulfate [C_2mim] [C_2SO_4] (see

Example 5.4) at high temperature to intensify the production process. For this purpose a micro heat exchanger with square channels as illustrated in Figure 5.25 should be used. The reactor channels are alternatively assembled with cooling channels of the same diameter. 50 stainless steel foils with 50 channels each are piled in between 51 foils with 50 cooling channels. In total 1250 reactor channels and 1300 cooling channels are assembled. Water is used as cooling medium. The walls of the channels have a thickness of $e = 100\,\mu m$.

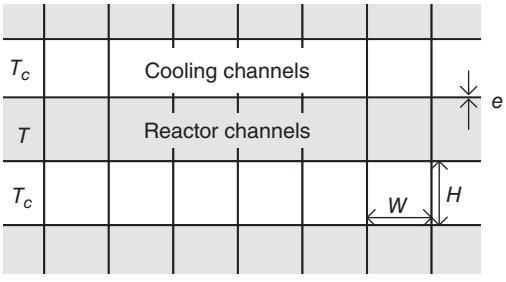

Figure 5.25 Micro heat exchanger for the synthesis of $[C_2mim]$ $[C_2SO_4]$. Total number of channels: 2550, reactor length $L_t = 0.2\,m$.

To avoid any risk of reactant or product degradation, the maximum hot spot temperature is fixed to $T_{max} = 95\,°C$.

The following operational parameters must be estimated for the final design of the reactor:

1) The cooling temperature $T_c = T_0$.
2) The mean residence time to get the required conversion of $X \geq 0.75$, supposing plug flow behavior in the channels.
3) The overall volumetric heat transfer coefficient, U_v.
4) The hydraulic channel diameter, which corresponds to the height of the channel ($d_h = H = W$).
5) The total throughput ($kg\,h^{-1}$) and the pressure drop in the channels.

Solution:

1) The cooling temperature can be estimated from the definition of the dimensionless maximum temperature: $\Delta T'_{max} = \frac{T_{max} - T_c}{T_c^2} \frac{E_a}{R} = 1.2$. With $T_{max} = 368\,K$ a cooling temperature of 353.5 K is calculated. For the safe reactor design we will take $T_c = T_0 = 353\,K$. The hot spot temperature is estimated to reach $T_{max} = 367.5\,K$.
2) To estimate the mean residence time in a plug flow reactor we suppose a constant reactor temperature. This leads to $DaI = \frac{\tau_R}{t_r} = \frac{X}{1-X}$; $\frac{\tau_R}{t_r} = \frac{0.75}{0.25} = 3$.

The characteristic reaction time is defined with the inlet condition.

$$t_r = \frac{1}{k(T_c)\cdot c_{1,0}} \Rightarrow t_{r,353} = \frac{1}{k_{313}\exp\left(-\frac{E_a}{R}\left(\frac{1}{353}-\frac{1}{313}\right)\right)\cdot 4.7} = 3.35\,\mathrm{s}$$

$$\tau_R = DaI \cdot t_r = 3 \cdot 3.35\,\mathrm{s} = 10\,\mathrm{s}$$

3) The estimation of the overall volumetric heat transfer coefficient is based on the relation in Equation 5.49:

$$N'_{\min} = \frac{t_r}{t_c} = 2.72 \cdot S' - 4.57 \cdot \sqrt{S'};\quad S' = \Delta T_{\mathrm{ad}} \frac{E_a}{R \cdot T_c^2};\quad t_c = \frac{\rho \cdot c_p}{U_v}$$

$$\Delta T_{\mathrm{ad}} = \frac{c_{1,0}(-\Delta H_r)}{\rho_{353} c_{p,353}} = \frac{4.7 \cdot 102{,}000}{1210 \cdot 1.73} = 229\,\mathrm{K}$$

$$S' = \Delta T_{\mathrm{ad}} \frac{E_a}{R \cdot T_c^2} = 229 \cdot \frac{86{,}000}{8.314 \cdot (353)^2} = 19$$

$$N'_{\min} = \frac{t_r}{t_c} = 2.72 \cdot 19 - 4.57 \cdot \sqrt{19} = 31.8 \Rightarrow t_c = \frac{t_r}{N'_{\min}} = 0.105\,\mathrm{s}$$

$$U_v = \frac{\rho \cdot c_p}{t_c} = \frac{1210 \cdot 1.73}{0.105} = 1.9910^4 \cong 2 \cdot 10^4\,\mathrm{kW\,m^{-3}\,K^{-1}}$$

4) To determine the hydraulic diameter of the channel, we will use the relationship given in Equation 5.33

$$\frac{1}{U} = \frac{1}{h_r} + R_{\mathrm{th}} = \frac{d_h}{Nu \cdot \lambda_f} + R_{\mathrm{th}} \Rightarrow U = C_{\mathrm{Rth}} \cdot h_r = C_{\mathrm{Rth}} \frac{Nu \cdot \lambda_f}{d_h}$$

The resistance to heat transfer in the channel walls is very low because of the small wall thickness of 100 µm and can be neglected in the further calculations: $R_{\mathrm{th}} \cong 1/h_{\mathrm{ex}} = d_h/(Nu \cdot \lambda_{f,\mathrm{ex}})$. We suppose established temperature and laminar velocity profile in the reactor and cooling channels. Therefore, the same asymptotic Nusselt number can be used. From Figure 5.4 we find $Nu_\infty = 3.7$ for square channels.

$$\frac{1}{U} = \frac{1}{h_r} + R_{\mathrm{th}} = \frac{d_h}{Nu \cdot \lambda_f} + \frac{d_h}{Nu \cdot \lambda_{f,c}};\quad U = \frac{Nu}{d_h}\left(\frac{1}{\lambda_f} + \frac{1}{\lambda_{f,c}}\right)^{-1}$$

$$U = C_{\mathrm{Rth}} \cdot h_r$$

$$\Rightarrow C_{\mathrm{Rth}} = \frac{U}{h_r} = \frac{1/\lambda_f}{1/\lambda_f + 1/\lambda_{f,c}} = \frac{1/0.18}{1/0.18 + 1/0.66} = 0.79$$

The heat conductivity of the cooling water at $T_c = 353\,\mathrm{K}$ is $\lambda_{f,c} = 0.66\,\mathrm{W\,m^{-1}\,K^{-1}}$ [8].

The overall volumetric heat transfer coefficient is given by $U_v = U \cdot \frac{A_{ex}}{V_R} = C_{Rth} \frac{Nu \cdot \lambda_f}{d_h} \cdot \frac{A_{ex}}{V_R}$ with $\frac{A_{ex}}{V_R} = \frac{2 \cdot H}{H^2} = \frac{2}{d_h}$ for channels cooled on two sides, it follows $U_v = C_{Rth} \frac{Nu \cdot \lambda_f}{d_h} \cdot \frac{2}{d_h} \Rightarrow d_h = \sqrt{C_{Rth} \frac{Nu \cdot \lambda_f \cdot 2}{U_v}}$

$$d_h = \sqrt{0.79 \frac{3.7 \cdot 0.18 \cdot 10^{-3} \cdot 2}{2 \cdot 10^{-4}}} = 229 \cong 230\,\mu m$$

5) The pressure drop in the reaction channels is given by the Hagen – Poisseuille law as

$$\Delta p = 32 \cdot \zeta \cdot \frac{u \cdot \mu}{d_h^2} L_t; \zeta = 0.89 \text{ for square channels; } \quad u = \frac{L_t}{\tau_R} = 0.02\,m\,s^{-1}$$

The viscosity of ([C_2mim] [C_2SO_4]) at 353 K is $\mu = 15.57 \quad 10^{-3}$ Pa s (Table 5.4)

$$\Delta p = 32 \cdot 0.89 \cdot \frac{0.02 \cdot 15.57 \cdot 10^{-3}}{(2.3 \cdot 10^{-4})^2} 0.2 = 3.35 \cdot 10^4\,Pa = 0.335\,bar$$

The mass flow through the channel is $\dot{m}_{channel} = \dot{V} \cdot \rho = u \cdot A_{cs} \cdot \rho = 0.02 \cdot (2.3 \cdot 10^{-4})^2 \cdot 1.21 \cdot 10^3 = 1.28 \cdot 10^{-6}\,kg\,s^{-1}$

Total mass flow: $\dot{m} = 1250 \cdot \dot{m}_{channel} = 1.6 \cdot 10^{-3}\,kg\,s^{-1} = 5.76\,kg\,h^{-1}$

5.3.3 Multi-injection Microstructured Reactors

As discussed in chapter 5.3.2, theoretically the temperature of every fast and exothermic reaction can be controlled in microchannel reactors. The simplest solution is to adapt the reactor dimensions according to the reaction properties like adiabatic temperature rise, characteristic reaction time, and activation energy, thus working under stable conditions (see Equation 5.49). By reducing channel diameter, the channel volume for constant reactor length decreases proportionally to diameter square. For exothermic quasi-instantaneous reactions, channel sizes below 100 µm may be needed, which cannot be operated on an industrial scale because of high friction losses and high risk to channel clogging.

For the described limits, one possible solution to combine high-throughput with good thermal management is a multi-injection microchannel reactor, where one reactant is injected along the reactor. This concept is used as one of the approaches for scale-up [34, 35]. Distributed feeding of one reactant in multiple locations reduces the local heat power released depending on the number of injection points. The concept corresponds to the semibatch operation of conventional reactor vessels.

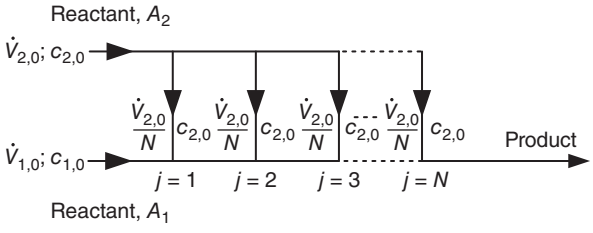

Figure 5.26 Scheme of a multi-injection reactor with *N* injection points.

5.3.3.1 **Mass and Energy Balance in Multi-injection Microstructured Reactors**

For a multi-injection MSR with a total of N injection points (Figure 5.26), the mass balance can be derived in a similar approach as for a plug flow reactor with only one inlet (Equation 5.27) [35].

The only difference is a sudden change in temperature and reaction mass at each injection point *j*, which can be described by using a Dirac pulse $\delta(z)$ and the Heaviside function $\sigma(z)$. Reactant A_2 contained in flow 2 is injected in deficit to reactant A_1 into flow 1 before reaching the last point, where the stoichiometric balance is attained. It is assumed that the volume of the injected reactant is equal at each injection point and that it mixes instantaneously with the main stream.

$$\frac{\mathrm{d}\dot{n}_i}{\mathrm{d}z} = A_{\mathrm{cs}} \cdot R_i + \delta\left(z - \frac{L_t}{N} \cdot (j-1)\right) \cdot \frac{\dot{n}_{2,0}}{N} \tag{5.53}$$

$$\begin{aligned}\frac{\mathrm{d}T}{\mathrm{d}z} = {} & A_{\mathrm{cs}} \cdot \frac{(-R_1) \cdot (-\Delta H_r)}{\left(\dot{V}_{1,0} + \sum_{j=1}^{N} \sigma\left(z - \frac{L_t}{N} \cdot (j-1)\right) \cdot \frac{\dot{V}_{2,0}}{N}\right) \cdot \overline{\rho} \cdot \overline{c}_p} \\ & - A_{\mathrm{cs}} \cdot \frac{U \cdot a \cdot (T - T_c)}{\left(\dot{V}_{1,0} + \sum_{j=1}^{N} \sigma\left(z - \frac{L_t}{N} \cdot (j-1)\right) \cdot \frac{\dot{V}_{2,0}}{N}\right) \cdot \overline{\rho} \cdot \overline{c}_P} \\ & + \delta\left(z - \frac{L_t}{N} \cdot (j-1)\right) \cdot \frac{\dot{V}_{2,0}}{\dot{V}_{1,0} \cdot N}(T_{\mathrm{inj}} - T)\end{aligned} \tag{5.54}$$

The third term of heat balance (Equation 5.54) is the heat added to the system because of the eventual temperature difference between the injected flow $\dot{V}_2$ and the main flow denoted as $(T_{\mathrm{inj}} - T)$. The above equations can be solved using a simple ordinary differential equation solver for each interval between two injection points. In this case, the boundary conditions of the *j*th interval have to be adapted considering the reaction mass injected at point *j* and its temperature as well as the temperature and concentrations at the end of the interval *j – 1*.

If instantaneous mixing and reactions are considered, the heat is produced at the injection point in the reactor. The heat evacuation time can be calculated by

following heat balance equation:

$$\frac{\mathrm{d}T}{\mathrm{d}\tau} = \frac{U \cdot a}{\rho c_p}(T_c - T) = \frac{U_v}{\rho c_p}(T_c - T) \tag{5.55}$$

Integration of Equation 5.55 allows to determine the residence time between two injection points (τ_j), respectively, the distance (L_j) to cool the reaction mass from $T_{\text{in},\,j}$ to $T_{\text{out},\,j}$ (Equation 5.56).

$$\begin{aligned} \tau_j &= \frac{\rho c_p}{U_{v,j}} \ln\left(\frac{T_{\text{in},j} - T_c}{T_{\text{out},j} - T_c}\right) \\ L_j &= \frac{\rho c_p u_j}{U_{v,j}} \ln\left(\frac{T_{\text{in},j} - T_c}{T_{\text{out},j} - T_c}\right) \end{aligned} \tag{5.56}$$

where u_j is the velocity at jth injection and $U_{v,\,j}$ the overall volumetric heat transfer coefficient in the jth section. The inlet temperature for each injection point differs and so does the outlet temperature. For the first injection, the inlet temperature is the sum of the cooling temperature and the adiabatic temperature rise at first point as given in the following:

$$T_{\text{in},1} = T_o + \Delta T_{\text{ad},1} = T_c + \Delta T_{\text{ad},1}; \quad \text{for } T_o = T_c \quad j = 1 \tag{5.57}$$

If we consider equal flow splitting for all injection points, the total volumetric flow rate and corresponding adiabatic temperature rise would be given as

$$\begin{aligned} \dot{V}_1 &= \dot{V}_{1,0} + \frac{\dot{V}_{2,0}}{N} \\ \Delta T_{\text{ad},1} &= \frac{(\dot{n}_{2,0}/N)(-\Delta H_r)}{(\rho \dot{V}_1) \cdot c_p} \end{aligned} \quad j = 1 \tag{5.58}$$

where $\dot{n}_{2,0}$ is the inlet molar flow rate of A_2 ($\dot{n}_{2,0} = \dot{V}_{2,0} \cdot c_{2,0}$). According to Equation 5.56, the residence time required to remove the heat completely ($T_{\text{out}} = T_c$) is infinity and, therefore, an adjustment needs to be made. If we assume that 90% of the heat is removed within one section and 10% will be carried to the next injection point, the corresponding outlet temperature can be calculated with Equation 5.59.

$$T_{\text{out},1} = T_c + 0.1(T_{\text{in},1} - T_c) \tag{5.59}$$

Further, temperature at the second injection for constant heat capacity is

$$\begin{aligned} T_{\text{in},2} &= \frac{\dot{V}_{1,0} + \dot{V}_{2,0}/N}{\dot{V}_{\text{tot},2}} T_{\text{out},1} + \frac{\dot{V}_{2,0}/N}{\dot{V}_{\text{tot},2}} T_c + \Delta T_{\text{ad},2} \\ &= \frac{\dot{V}_1}{\dot{V}_{\text{tot},2}} T_{\text{out},1} + \frac{\dot{V}_{2,0}/N}{\dot{V}_{\text{tot},2}} T_c + \Delta T_{\text{ad},2} \end{aligned} \tag{5.60}$$

and

$$\dot{V}_{\text{tot},2} = \dot{V}_{1,0} + 2\frac{\dot{V}_{2,0}}{N};\quad \Delta T_{\text{ad},2} = \frac{(\dot{n}_{2,0}/N)(-\Delta H_r)}{(\rho\,\dot{V}_{\text{tot},2})\cdot c_p} \tag{5.61}$$

For a multi-injection MSR with equal injection at all points, a generalized equation can be established to investigate the temperature at *j*th injection:

$$T_{\text{in},j} = \frac{\dot{V}_{j-1}}{\dot{V}_j}T_{\text{out},j-1} + \frac{\dot{V}_{2,0}/N}{\dot{V}_j}T_c + \Delta T_{\text{ad},j};\quad \Delta T_{\text{ad},j} = \frac{(\dot{n}_{2,0}/N)(-\Delta H_r)}{(\rho\,\dot{V}_j)\cdot c_p} \tag{5.62}$$

with $\dot{V}_j = \dot{V}_{1,0} + j\cdot\frac{\dot{V}_{2,0}}{N}$. The axial temperature profile in multi-injection microchannels is presented in Example 5.6.

Example 5.6: Characteristics of a multi-injection microchannel reactor

A second order quasi-instantaneous reaction (heat of reaction = $-120\,000\,\text{kJ kmol}^{-1}$) is carried out in a microstructured plug flow reactor. To reduce the hot spot temperature, the reaction partner, $A_{2,}$ is evenly distributed over several injection points along the reactor length. The reactor conditions and properties are summarized in Table 5.5:

Table 5.5 Physical properties and reaction condition.

Reaction enthalpy	$\Delta H_\text{r} = -120\,000\,\text{kJ kmol}^{-1}$
Density	$\rho = 1142\,\text{kg m}^{-3}$
Specific heat capacity	$c_p = 1.7\,\text{kJ kg}^{-1}\,\text{K}^{-1}$
Inlet concentrations	$c_{1,0} = c_{2,0} = 1.56\,\text{kmol m}^{-3}$
Inlet flow rate	$\dot{V}_{1,0} = \dot{V}_{2,0} = 0.9\cdot 10^{-7}\,\text{m}^3\,\text{s}^{-1}$

Considering three configurations of 4, 6, and 10 injections and assuming instantaneous mixing at each contacting junction, investigate the adiabatic temperature rise for each injection point.

Solution:

The total adiabatic temperature rise (ΔT_{ad}) is given as

$$\Delta T_{\text{ad}} = \frac{\dot{n}_{2,0}(-\Delta H_r)}{(\dot{V}_{1,0}+\dot{V}_{2,0})\cdot\rho c_P} = \frac{1.4\times 10^{-7}\times 120000}{1142\times 0.18\times 10^{-6}\times 1.7} = 48.08\,\text{K} \tag{5.63}$$

The adiabatic temperature rise corresponding to total concentrations is 48.08 K. Let us consider an MSR with four injection points ($N = 4$); the flow rate and adiabatic temperature rise at each injection is given by Equation 5.62 (Table 5.6).

Table 5.6 Temperature rise at different injection point in multi-injection reactor.

Injection point	$N = 6$		$N = 10$	
	$\dot{V}_j$ ($m^3\ s^{-1}$)	$\Delta T_{ad,j}$ (K)	$\dot{V}_j$ ($m^3\ s^{-1}$)	$\Delta T_{ad,j}$ (K)
1	1.05×10^{-7}	14.3	9.90×10^{-8}	9.1
2	1.20×10^{-7}	12.5	1.08×10^{-7}	8.35
3	1.35×10^{-7}	11.1	1.17×10^{-7}	7.70
4	1.50×10^{-7}	10	1.26×10^{-7}	7.15
5	1.65×10^{-7}	9.1	1.35×10^{-7}	6.68
6	1.80×10^{-7}	8.35	1.44×10^{-7}	6.26
7	—	—	1.53×10^{-7}	5.89
8	—	—	1.62×10^{-7}	5.56
9	—	—	1.71×10^{-7}	5.27
10	—	—	1.80×10^{-7}	5.01

For injection $j = 1$:

$$\dot{V}_1 = 0.9 \times 10^{-7} + 1\frac{0.9 \cdot 10^{-7}}{4} = 1.125 \times 10^{-7}\,m^3\,s^{-1}$$

$$\Delta T_{ad,1} = \frac{(1.4 \times 10^{-7}/4) \times 120000}{1142 \cdot 1.125 \cdot 10^{-7} \cdot 1.7} = 19.23\,K$$

Similarly, for injection point $j = 2$:

$$\dot{V}_1 = 1.35 \cdot 10^{-7}\,m^3\,s^{-1};\ \ \Delta T_{ad,2} = 16.02\,K$$

For injection $j = 3$:

$$\dot{V}_1 = 1.57 \cdot 10^{-7}\,m^3\,s^{-1};\ \ \Delta T_{ad,2} = 13.77\,K$$

For injection $j = 4$:

$$\dot{V}_1 = 1.80 \cdot 10^{-7}\,m^3\,s^{-1};\ \ \Delta T_{ad,2} = 12.01\,K$$

The temperature rise at each injection point decreases along the length of the reactor because of the increase in the flow rate.

In spite of the fact that in multi-injection microchannels the temperature profiles are not well established because of the injection along the length that disturbs each time the velocity and temperature profile increasing the heat transfer performance, we use a constant overall volumetric heat transfer coefficients for simplicity. Keeping the residence time in each section constant, the outlet temperatures in each section are identical (see Equation 5.56). But, because of the increasing volumetric flow, the lengths of the sections vary as shown in Figure 5.27.

Practically, the mixing at the injection point is not instantaneous. The rates of fast reactions are influenced by mixing. The mixing time varies from milliseconds

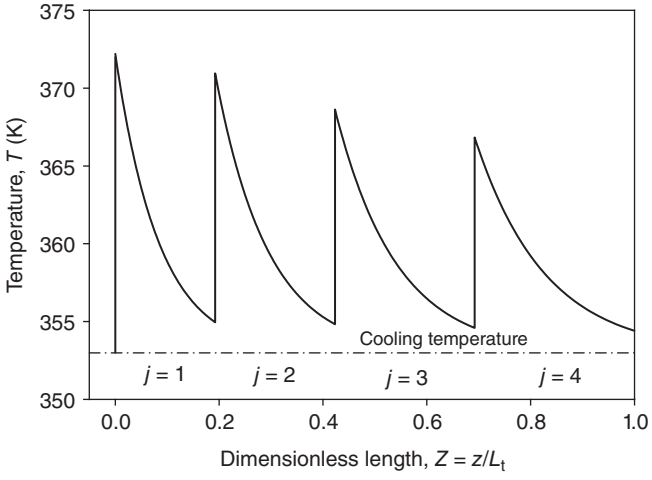

Figure 5.27 Typical temperature profile in a multi-injection microchannel ($N = 4$). Ninety percentage of the heat produced at each injection is removed within each section j.

to a few seconds (Chapter 4); therefore, in practice a significant amount of time should be considered for mixing and then for heat evacuation.

The influence of the transformation rate, respectively the characteristic reaction time on the temperature profile in multi-injection reactors, is shown in Figure 5.28 for a second order reaction. For nearly all instantaneous reactions, the

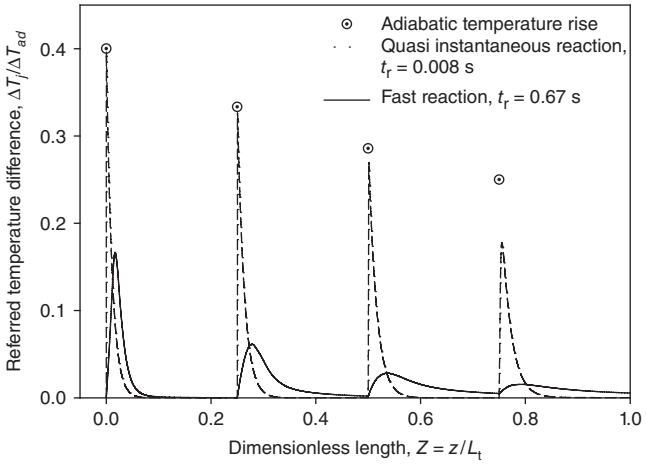

Figure 5.28 Temperature profile in a multi-injection reactor with $N = 4$ injection points. Influence of the effective characteristic reaction time. $T_0 = T_{inj} = T_c$.

maximum temperature at the first injection points reaches the values predicted with Equations 5.58 and 5.62. Because of the decreasing concentrations of reactant A_1 and the dilution following the injected flow 2, the reaction rate diminishes and the predicted temperature rise at the fourth injection point is not attained. For a fast reaction with a characteristic reaction time of 0.67 s the maximum temperature is considerably lower than the adiabatic temperature. Because of the high overall volumetric heat transfer coefficient, efficient heat evacuation in the mixing zone reduces the hot spot temperature.

5.3.3.2 Reduction of Hot Spot in Multi-injection Reactors

Number of Injection Points The hot spot within a multi-injection reactor is controlled mainly by the amount of injection points (N). For a first approximation of the temperature rise at each injection point, a simplified system can be considered [34]. For the case of instantaneous mixing and reaction with an equally distributed flow among the injection points ($\dot{V}_{2,1} = \dot{V}_{2,2} = \cdots = \dot{V}_{2,N} = \dot{V}_{2,0}/N$), the temperature rises quasi-adiabatically at each injection point. In order to avoid a high temperature rise, the heat produced at each injection point j is removed before reaching the next injection point $j+1$. For such a system, Equation 5.62 can be rewritten as

$$\Delta T_{\mathrm{ad},j} = \frac{(\dot{V}_{2,0}/N)}{(\dot{V}_{1,0} + j(\dot{V}_{2,0}/N))} \frac{c_{2,0} \cdot |-\Delta H_r|}{\overline{\rho} \cdot \overline{c}_p} = \frac{1}{\left(N \cdot \frac{\dot{V}_{1,0}}{\dot{V}_{2,0}} + j\right)} \cdot \frac{c_{2,0} \cdot |\Delta H|}{\overline{\rho} \cdot \overline{c}_p} \quad (5.64)$$

The adiabatic temperature rise for a single-injection reactor (ΔT_{ad}) is defined as

$$\Delta T_{\mathrm{ad}} = \frac{\dot{V}_{2,0} \cdot c_{2,0} \cdot (-\Delta H_r)}{(\dot{V}_{1,0} + \dot{V}_{2,0})\overline{\rho} \cdot \overline{c}_p} \quad (5.65)$$

The temperature rise at each injection point referred to the adiabatic temperature rise obtained in reactors with only one inlet ($N = 1$) is expressed in Equation 5.66.

$$\frac{\Delta T_{\mathrm{ad},j}}{\Delta T_{\mathrm{ad}}} = \frac{\left(\frac{\dot{V}_{1,0}}{\dot{V}_{2,0}} + 1\right)}{\left(N \cdot \frac{\dot{V}_{1,0}}{\dot{V}_{2,0}} + j\right)} \quad (5.66)$$

It is obvious that the highest temperature rise occurs at the first injection point as shown in Figure 5.29.

A further reduction in hot spot can be obtained by maximizing the flow ratio $\dot{V}_{2,0}/\dot{V}_{1,0}$. The influence of the number of injection point and the ratio $\dot{V}_{2,0}/\dot{V}_{1,0}$ is shown in Figure 5.29. To apply the simple relation (Equation 5.66), one has to choose carefully the distances between consecutive injection points to avoid the accumulation of heat in the reactor (see Equation 5.55).

Rewriting Equation 5.66, the maximum number of injection points required to avoid a temperature rise higher than $\Delta T_{\mathrm{ad},\,N,\,j=1}$ can be estimated as a function of $F = \dot{V}_{2,0}/\dot{V}_{1,0}$ and the adiabatic temperature rise of the reaction $\Delta T_{\mathrm{ad},\,N=1}$ in the

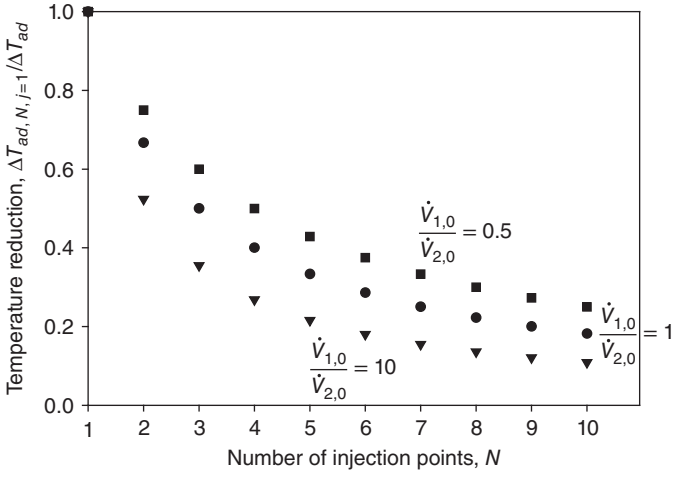

Figure 5.29 Reduction of temperature rise at the first injection point ($j = 1$) as a function of the total amount of injection points N and inlet flow ratios $F = \dot{V}_{2,0}/\dot{V}_{1,0}$.

case of a single injection point reactor ($N = j = 1$):

$$N = (1 + F)\frac{\Delta T_{\mathrm{ad},N=1}}{\Delta T_{\mathrm{ad},N,j=1}} - F; \text{with } F = \frac{\dot{V}_{2,0}}{\dot{V}_{1,0}} \tag{5.67}$$

Again, one has to choose carefully the characteristic cooling time to avoid the accumulation of heat in the reactor.

Unequal Flow Partition In the previous sections, the flow through the injection channels was assumed to be equal. It was shown that this type of design results in a temperature profile as given in Figure 5.27, which leads to a maximum temperature at the first injection point. In order to further reduce this maximum temperature in a multi-injection reactor, one can design a microchannel reactor to obtain N equally high hot spots by increasing the injected volume along the length. The optimal flow distribution can be calculated using the model above. For a multi-injection reactor with N injection points, the adiabatic temperature rise at each injection point has to be equal as

$$\Delta T_{\mathrm{ad},N,1} \overset{(1)}{=} \Delta T_{\mathrm{ad},N,2} \overset{(2)}{=} \Delta T_{\mathrm{ad},N,3} \overset{(3)}{=} \ldots \overset{(N-1)}{=} \Delta T_{\mathrm{ad},N,N} \tag{5.68}$$

It leads to a set of $N - 1$ equations for N unknown normalized injection flow rates $F_j = \dot{V}_{2,j}/\dot{V}_{1,0}$. Solving Equation 5.68 leads to the following expression for the normalized injection flow rates as a function of F_1:

$$F_j = F_1 \cdot (F_1 + 1)^{j-1} \tag{5.69}$$

Thus the growth factor for the volumetric flow rate between two injection points j and $j+1$ is $(F_1 + 1)$. Assuming a constant density along the length:

$$F = \sum_{j=1}^{N} F_j \tag{5.70}$$

From above equation, F_j can be determined for a known value of F. Using above example ($F = 1$ and $N = 4$), the injection flow rate at $j = 1$ is $F_1 = 0.182$ resulting in a growth factor of 1.182. The adiabatic temperature rise at any injection point can be calculated according to Equation 5.64:

$$\Delta T_{\mathrm{ad},N,j} = \Delta T_{\mathrm{ad},N,1} = \frac{\dot{V}_{2,1}}{(\dot{V}_{1,0} + \dot{V}_{2,1})} \frac{c_{2,0} \cdot (-\Delta H_r)}{\rho \cdot \bar{c}_p} = \frac{F_1}{1 + F_1} \cdot \frac{c_{2,0} \cdot (-\Delta H_r)}{\rho \cdot \bar{c}_p} \tag{5.71}$$

The adiabatic temperature rise for a single-injection reactor (ΔT_{ad}) is calculated with Equation 5.65. Thus, the temperature rise at each injection point referred to the adiabatic temperature rise obtained in reactors with only one inlet ($N = 1$) is expressed in Equation 5.72

$$\frac{\Delta T_{\mathrm{ad},N,j}}{\Delta T_{\mathrm{ad}}} = \frac{\Delta T_{\mathrm{ad},N,1}}{\Delta T_{\mathrm{ad}}} = \frac{\dot{V}_{2,1}}{\dot{V}_{1,0} + \dot{V}_{2,1}} \frac{\dot{V}_{1,0} + \dot{V}_{2,1}}{\dot{V}_{2,0}} = \frac{F_1}{1 + F_1} \frac{1 + F}{F} \tag{5.72}$$

Compared to an equally distributed multi-injection reactor with $N = 4$ a 20% reduced temperature rise at the first injection point is obtained. Especially in cases with high F, this kind of channel design can be beneficial (see Example 5.7).

Example 5.7: Multi-injection microtubular reactor with identical temperature rises.

The reaction described in Example 5.6 can be carried out in a microtubular reactor with $N = 2$ injections. Identical adiabatic temperature rises are required ($\Delta T_{\mathrm{ad},2,1} = \Delta T_{\mathrm{ad},2,2}$). Determine the injecting flows $\dot{V}_{2,1}$, $\dot{V}_{2,2}$ and the resulting adiabatic temperature rise. Estimate the reactor length to evacuate 90% of the produced heat (Table 5.7).

Table 5.7 Physical properties and reaction condition.

Reaction enthalpy	$\Delta H_r = -120\,000\ \mathrm{kJ\ kmol^{-1}}$
Density	$\rho = 1142\ \mathrm{kg\ m^{-3}}$
Specific heat capacity	$c_p = 1.7\ \mathrm{kJ\ kg^{-1}\ K^{-1}}$
Inlet concentrations	$c_{2,0} = 2.33\ \mathrm{kmol\ m^{-3}}$; $c_{1,0} = 5\ \mathrm{kmol\ m^{-3}}$
Inlet flow rate	$\dot{V}_{1,0} = 1.2 \cdot 10^{-7}\ \mathrm{m^3\ s^{-1}}$; $\dot{V}_{2,0} = 0.6 \cdot 10^{-7}\ \mathrm{m^3\ s^{-1}}$
Tubular reactor	$d_t = 1\ \mathrm{mm}$
Volumetric heat transfer coefficient	$U_v = 1464\ \mathrm{kW\ m^{-3}\ K^{-1}}$

Solution:

The ratio between inlet flow 2 to 1 is $F = \dot{V}_{2,0}/\dot{V}_{1,0} = 0.6/1.2 = 0.5$. From Equations 5.70 and 5.69 follows:

$$F = F_1 + F_2 = F_1 + F_1(F_1 + 1) = 0.5; \Rightarrow F_1 = 0.225$$

$$F_2 = F_1(F_1 + 1) = 0.276$$

$$\Delta T_{\mathrm{ad},2,1} = \Delta T_{\mathrm{ad},2,2} = \frac{F_1}{1+F_1}\frac{1+F}{F}\Delta T_{\mathrm{ad}};\quad \frac{0.225}{1.225}\frac{1.5}{0.5}\cdot 48 = 26.5\,\mathrm{K}$$

5.4
Case Studies

Three examples of new designs of single-injection MSR and one example of multi-injection reactor applied for fast and exothermic liquid phase reactions are presented. Finally, it is demonstrated that the process intensification has been achieved using these microreactors.

5.4.1
Synthesis of 1,3-Dimethylimidazolium-Triflate

This is a quasi-instantaneous second order reaction (Figure 5.30) [36]. The important characteristic of this reaction is that at temperatures above 100 °C, product coloration is observed indicating its decomposition and hence has to be avoided. A cooling system was integrated in the MSR and toluene was used as a coolant. Because of its low boiling point, toluene evaporates creating an additional effect on channel wall (two-phase cooling). The evaporated coolant is condensed in a 120 W-heat pipe system, which is normally used for cooling the CPU unit of computer. Because the reaction is of the second order, the highest heat production occurs in the mixer located at the entrance of the residence time loop. Temperature is monitored by two thermocouples placed on the outer surface of the static mixer and the reactor outlet, respectively. The maximum tolerable temperature

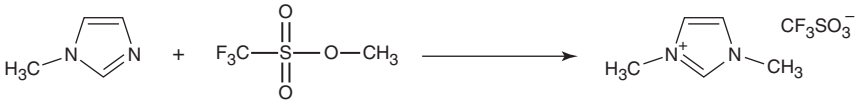

Figure 5.30 Reaction scheme for the synthesis of the ionic liquid 1,3-Dimethylimidazolium-triflate [36].

is given by reactant 2 (see Figure 5.30) whose boiling point lies at 100 °C. When MSR is working just under ambient cooling (natural convection/heat conduction), the maximal attainable flow rate lies at about 0.6 ml min^{-1}. The total flow rate was increased up to 9.7 ml min^{-1} by applying the two-phase cooling and thus confirming significant process intensification.

5.4.2
Nitration of Dialkyl-Substituted Thioureas

The target product is symmetrically substituted *N,N′*-dialkyl-*N,N′*-dinitro-urea, which is conventionally obtained at yields of about 10% (Figure 5.31) [37]. The reaction was carried out in silicon MSR with channels of 250 µm width. In order to increase the throughput, after the mixing of both reactants, the initial flow was distributed to nine identical channels cooled from both sides.

The temperature gradient inside the channels was monitored by the means of infrared thermometry (see Figure 5.32). Because of the small channel size and

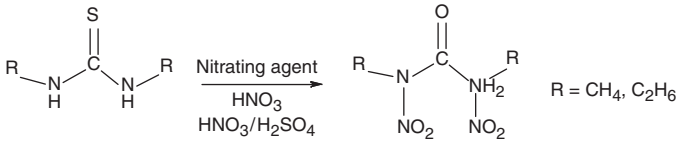

Figure 5.31 Nitration of dialkyl substituted thio-urea.

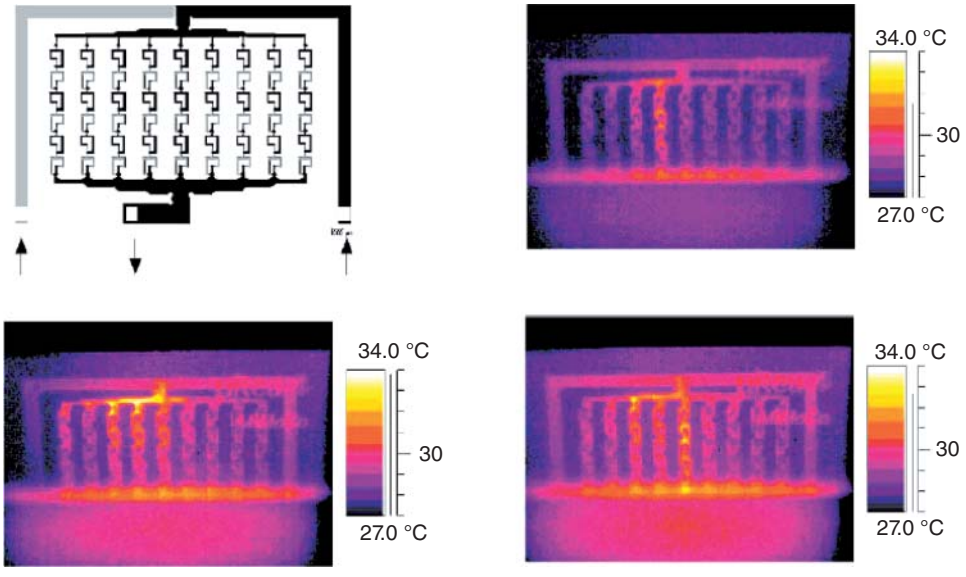

Figure 5.32 Infrared thermometry of the microreactor used to carry out nitration of dialkyl-substituted thioureas [37]. (Adapted with permission from Elsevier.)

the relatively high thermal conductivity of silicon ($\lambda = 148\ \mathrm{W\ mK^{-1}}$), temperatures inside the channel were almost the same (close to the isothermal operation). The temperature rise at the hot spot was about 5 °C and it was mostly located in the section for distributing the liquids to the channels and in the collecting part. This example demonstrates that by changing the mixers from macro to micro scale, the mixing properties as well as the temperature control of this exothermic reaction was improved allowing a close to isothermal operation and resulting in the yield increase from 10 up to 85% at a residence time of 3 min.

5.4.3
Reduction of Methyl Butyrate

In this reaction, the initial reactant methyl butyrate is reduced by diisobutylaluminum hydride (Dibal-H) toluene to an unstable organometallic intermediate [38]. In a second step, the intermediate is further reduced to butyraldehyde, which is the desired product. A further reduction leads to the unwanted formation of butanol (Figure 5.33).

The reaction scheme can be simplified to:

$$\mathrm{A} \xrightarrow[\text{Dibal-H,toluene}]{k_1} \mathrm{B^*} \xrightarrow{k_2} \mathrm{C} \xrightarrow[\text{Dibal-H}]{k_3} \mathrm{D} \tag{5.73}$$

In this reaction, the rate constant $k_1 > k_2$. As the carbonyl group of aldehydes (C) is more reactive than that of esters (A), the rate constant $k_3 > k_1 > k_2$. Hence, the concentration of the target product C is very low during the reaction, which is usually carried out at low temperatures (around 238 K). In addition, B* is unstable at higher temperatures, which considerably reduces the yield of C at higher temperatures in batch mode. Because of the high exothermicity of the reaction and its instantaneous character, its implementation in an industrial scale using conventional semibatch reactor would result in extremely high dosing times and thus poor performance. Therefore, an MSR with four different mixing properties and cooling capacities were used [38].

This consecutive reaction shows high sensitivity to mixing as well as to temperature variations. Whereas in a lab-scale batch reactor 63% of the target product C is obtained only at temperatures lower than 218 K, similar selectivity

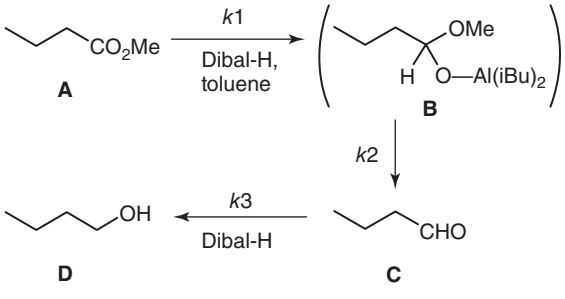

Figure 5.33 Reaction scheme of the reduction of methyl butyrate [38].

could be obtained in MSR for higher temperatures (up to 253 K) following an improved thermal control. It was shown that better yields are obtained by injecting the reactant at several points along reactor length. In this case, the single hot spot is divided in several hot spots. At temperatures above 253 K, the reaction rates are increased to a point where characteristic reaction time is lower than characteristic mixing time. In this regime, the yield becomes a function of the mixing properties of the reactor. The comparison of four MSR showed the best selectivity (90% surface area of product C in the gas chromatograph), which were obtained with ER-25 MSR at 218 K, which is a multilamination mixer with sheets of 25 µm opening and is equipped with integrated cooling. Lower yields were obtained with micromixers without integrated cooling or with longer characteristic mixing times.

5.4.4
Reactions with Grignard Reagent in Multi-injection Reactor

The reactions of this class are instantaneous (mixing controlled) and highly exothermic and so the selectivity is sensitive to mixing and temperature control [23, 34]. In the reaction involving organometallic reagents, phenylethyl magnesium bromide, and 2-chloropropionylchloride, a productivity of about 100 g min^{-1} was achieved in a 35 mm^3 continuous multi-injection reactor. It requires a batch reactor with 1 m^3 volume. The glass reactor (Figure 5.34) was

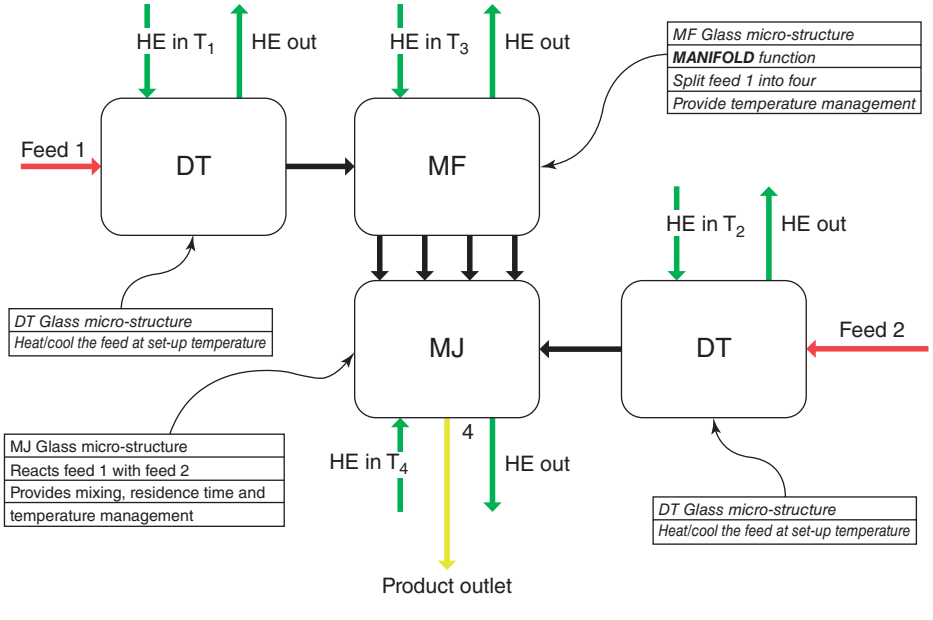

Figure 5.34 Scheme of a modular multi-injection reactor [34]. (Adapted with permission from Wiley.)

designed in a modular flexible manner for use in multiple processes. For each specific function required for an optimal performance in a multi-injection reactor, a separate module was built:

- *DT:* precooling of the feed.
- *MF:* flow distribution, splitting one flow into four using channel length to create equal pressure drop. Equal flow distribution is attained by ±8% relative variation.
- *MJ:* multi-injection unit, containing four injection points. Each injection point is followed by a mixing zone containing mixing elements. Each mixing zone leads into a residence time channel of 5 mm width, 0.6 m height, and 0.8 m length designed to evacuate the heat produced before reaching the following injection point. It has to be highlighted that the different zones in the multi-injection unit specifically avoid an unwanted temperature rise and accumulation of reactants.

In further experiments with the model Grignard reaction it was demonstrated that the increased number of injection points, N, increases the yield (Figure 5.35) [23]. The biggest gain in the yield (an increase from 22 to 30%) is obtained by switching from one injection point to two injection points. By adding more injection points, the relative yield increase diminishes. An increase of the number of injection points to more than six results in a maximum yield (of 37%). By repeating the same experiments with insufficient cooling between the injection points, a clear loss of selectivity can be seen. In order to increase the heat produced at each injection point, the flow rate is doubled from 18 to 36 g min^{-1} resulting in a further drop in yield down to 32% with six injection points. An identical behavior to that of low flow rate for insufficient cooling was observed at high flow rates.

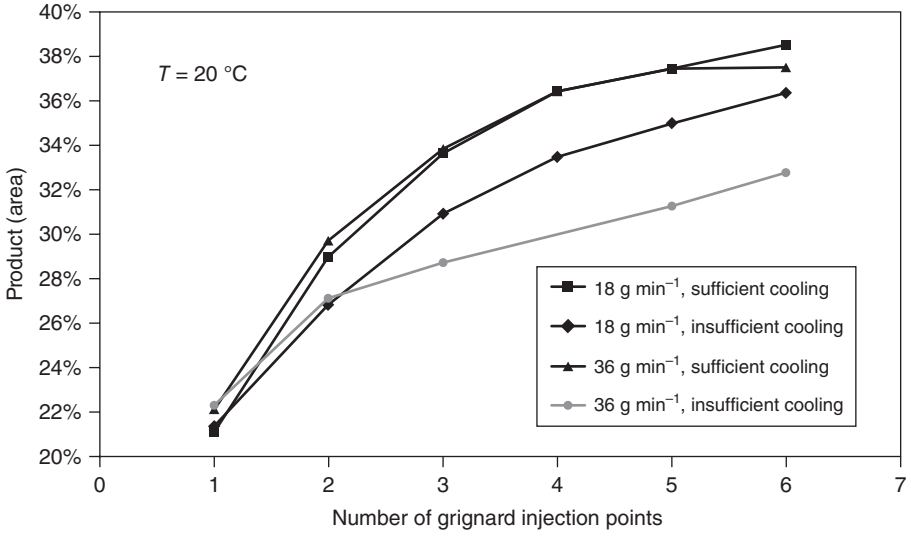

Figure 5.35 Effect of the number of injection points and cooling on product formation [23]. (Adapted with permission from Wiley.)

5.5 Summary

In this chapter, the general design criteria of MSR for fast and highly exothermic reaction are presented. For most reactions with characteristic reaction time over a few minutes, the temperature profile in MSR can be considered as nearly isothermal. For fast reactions with characteristic reaction time <1 min and with high reaction enthalpy, hot spots may be formed even in typical MSR. The rate of the heat release for this kind of reactions is partly or sometimes totally controlled by mixing. In order to avoid temperature rise in these cases, channel diameters of MSR are reduced, which can have two adverse effects: (i) small channels are sensitive to clogging resulting in runaway (ii) the number of units needed to reach the production target by numbering-up increases with the square of the channel diameter affecting the cost.

The multi-injection reactor concept is a valuable alternative allowing a good temperature control by injecting the limiting reactant along the reactor length. Different ways of decreasing hot spot magnitude in multi-injection reactor were shown: increasing the number of injection points, using the flow with the lowest heat capacity as injecting flow (maximizing F), and increasing the injected flow rates along the axial coordinate. For a maximum tolerable temperature rise, this concept allows working with higher channel diameter as compared to single-injection MSR, thus decreasing the number of units needed for numbering up.

In order to work safely with multi-injection reactor, an accumulation of the limiting reactant and of heat in the main channel has to be thoroughly prevented. As the considered reactions are mostly limited by mixing, the time required to mix can be estimated by using the correlation between specific energy dissipation and mixing time. Sufficient residence time should be provided between two injection points to minimize the hot spot.

5.6 List of Symbols

$A_{\mathrm{eff,ch}}$, A_{HEX}, A_{ref}	Effective heat exchange area, active heat exchange area, Reference area	m^2
a_{ref}	Specific reference area	$\mathrm{m}^2\,\mathrm{m}^{-3}$
a_w	Amplitudes of the wall waviness	—
C_{Rth}	Ratio of overall heat transfer coefficient to heat transfer coefficient in the reactor channel	—
e, e_{sw}	Wall thickness of the channels	m
F	Normalized injection flow rate	—

h_c, h_r, h_{wall}	Heat transfer coefficient of cooling medium, of reaction medium, of wall	$\mathrm{W\,m^{-2}\,K^{-1}}$
j	Injection number in multi-injection reactor	—
Kn	Knudsen coefficient	—
L_{circ}	Perimeter	m
l_{char}	Characteristic length	m
$L_{p,\,v}$	Specific reactor performance	$\mathrm{mol\,m^{-3}\,s^{-1}}$
m	Molecular mass	$\mathrm{g\,mol^{-1}}$
N	Number of parallel channels or injection points	—
N'	Ratio of the characteristic reaction time to the cooling time	—
Nu_m, Nu_∞, Nu_{seg}	Mean Nusselt number over the channel length, asymptotic value of Nusselt number, Nusselt number of segmented flow	—
Pr_L	Prandtl number of liquid phase	—
$\dot{Q}_c$, $\dot{Q}_{\text{ex}}$, $\dot{Q}_r$	Rate of energy exchange by convection, rate of energy exchange with surroundings, heat of energy produced by reaction	—
$\dot{q}_r$, $\dot{q}_{\text{ex}}$	Specific heat production, heat exchange	$\mathrm{J\,m^{-3}\,s^{-1}}$
Re_c, Re_r, Re_{Ls}	Reynolds number of cooling medium/fluid, of reaction mixture, of liquid slugs in multiphase flow	—
R_{th}	Heat transfer resistance	$\mathrm{m^2K\,W^{-1}}$
S'	Heat production potential	—
Se	Semenov number	—
t_{mr}	Time to maximum rate under adiabatic condition for zero order reaction	s
u_b, u_L	Linear velocity of gas bubble (slug), of liquid phase,	$\mathrm{m\,s^{-1}}$
u, u_c, u_r	mean velocity, of cooling medium/fluid, of reaction mixture	$\mathrm{m\,s^{-1}}$
$\delta(z)$	Dirac pulse	—
$\Delta T'$, $\Delta T'_{\text{max}}$	Dimensionless temperature difference, maximum temperature difference for safe operation	—
λ''	Wall corrugation wave length	m?
γ'	Aspect ratio	—
γ	Arrhenius numbers	—
λ_f, $\lambda_{f,\,c}$, λ_{wall}	Thermal conductivity of fluid, of the cooling fluid, of wall	$\mathrm{W\,m^{-1}\,K^{-1}}$
λ'	Mean free path of molecules	m
σ	Molecular length	m
η_{HEX}	Efficiency of heat exchanger	—
η_{sw}	Efficiency factor	—
$\sigma(z)$	Heaviside function	—
τ'	Molecular time scale	s
τ'_R	Dimensionless residence time	—

References

1. Gad-el-Hak, M. (1999) The fluid mechanics of microdevices - the Freeman scholar lecture. *J. Fluid Eng.-T ASME*, **121** (1), 5–33.
2. Jennings, S.G. (1988) The mean free path in air. *J. Aerosol Sci.*, **19** (2), 159–166.
3. Loose, W.A. and Hess, S. (1989) Rheology of dense fluids via nonequilibrium molecular hydrodynamics: shear thinning and ordering transition. *Rheol. Acta*, **28**, 91–101.
4. Bau, H.H. (1994) Transport processes associated with micro-devices. *Therm. Sci. Eng.*, **2**, 172–178.
5. Pfahler, J., Harley, J., Bau, H., and Zemel, J.N. (1991) Gas and liquid flow in small channels. Symposium on Micromechanical Sensors, Actuators, and Systems, 1991, ASME DSC-Vol. 32, pp. 49–60.
6. Pfahler, J., Harley, J., Bau, H., and Zemel, J. (1989) Liquid transport in micron and submicron channels. *Sens. Actuators, A*, **22** (1-3), 431–434.
7. Grote, K.-H. and Feldhusen, J. (2005) *Dubbel – Taschenbuch für den Maschinenbau*, 21st edn, Springer, Berlin, Heidelberg, New York.
8. (2002) *VDI-Wäarmeatlas*, 9 edn, Verein Deutscher Ingenieure, Springer, Berlin, Heidelberg, New York, Düsseldorf VDI-Verlag GmbH.
9. Cybulski, A. and Moulijn, J.A. (1994) Monoliths in heterogeneous catalysis. *Catal. Rev. Sci. Eng.*, **36** (2), 179–270.
10. Hartnett, J.P. and Kostic, M. (1989) Heat Transfer to Newtonian and Non-Newtonian Fluids in Rectangular Ducts, pp. 247–356.
11. Harris, C., Despa, M., and Kelly, K. (2000) Design and fabrication of a cross flow micro heat exchanger. *J. Microelectromech. Syst.*, **9** (4), 502–508.
12. Kockmann, N. (2008) Transport phenomena in micro process engineering, in *Heat and Mass Transfer* (eds D. Mewes and F. Mayinger), Springer, Berlin etc.
13. Shah, R.K. and Mueller, A.C. (2012) *Ullmann's Encyclopedia of Industrial Chemistry*, Wiley-VCH Verlag GmbH, Weinheim, pp. 309–419.
14. Wakami, H. and Yoshida, J.-i. (2005) Grignard exchange reaction using a microflow system: from bench to pilot plant. *Org. Process Res. Dev.*, **9** (6), 787–791.
15. Metwally, H.M. and Manglik, R.M. (2004) Enhanced heat transfer due to curvature-induced lateral vortices in laminar flows in sinusoidal corrugated-plate channels. *Int. J. Heat Mass Transfer*, **47** (10–11), 2283–2292.
16. Kockmann, N. and Roberge, D.M. (2009) Harsh reaction conditions in continuous-flow microreactors for pharmaceutical production. *Chem. Eng. Technol.*, **32** (11), 1682–1694.
17. Kockmann, N. and Roberge, D.M. (2011) Scale-up concept for modular microstructured reactors based on mixing, heat transfer, and reactor safety. *Chem. Eng. Process.*, **50** (10), 1017–1026.
18. Stief, T., Langer, O.-U., and Schubert, K. (1999) Numerical investigations of optimal heat conductivity in micro heat exchangers. *Chem. Eng. Technol.*, **22** (4), 297–303.
19. Lakehal, D., Larrignon, G., and Narayanan, C. (2008) Computational heat transfer and two-phase flow topology in miniature tubes. *Microfluid. Nanofluid.*, **4** (4), 261–271.
20. Betz, A.R. and Attinger, D. (2010) Can segmented flow enhance heat transfer in microchannel heat sinks? *Int. J. Heat Mass Transfer*, **53** (19-20), 3683–3691.
21. Asthana, A., Zinovik, I., Weinmueller, C., and Poulikakos, D. (2011) Significant Nusselt number increase in microchannels with a segmented flow of two immiscible liquids: An experimental study. *Int. J. Heat Mass Transfer*, **54** (7-8), 1456–1464.
22. Roberge, D.M. (2004) An integrated approach combining reaction engineering and design of experiments for optimizing reactions. *Org. Process Res. Dev.*, **8** (6), 1049–1053.
23. Roberge, D.M., Bieler, N., Mathier, M., Eyholzer, M., Zimmermann, B., Barthe, P., Guermeur, C., Lobet, O., Moreno, M., and Woehl, P. (2008) Development of an industrial multi-injection

microreactor for fast and exothermic reactions – Part II. *Chem. Eng. Technol.*, **31** (8), 1155–1161.

24. Anxionnaz, Z., Cabassud, M., Gourdon, C., and Tochon, P. (2008) Heat exchanger/reactors (HEX reactors): concepts, technologies: state-of-the-art. *Chem. Eng. Process.*, **47** (12), 2029–2050.
25. Barkelew, C.H. (1959) Stability of chemical reactors. *AIChE Symp. Ser.*, **55** (25), 38–46.
26. Baerns, M., Behr, A., Brehm, A., Gmehling, J., Hofmann, H., Onken, U., and Renken, A. (2006) *Technische Chemie*, 4th edn, Wiley-VCH Verlag GmbH, Weinheim, p. 733p.
27. Renken, A. (2006) in *Technische Chemie* (eds M. Baerns, A. Behr, A. Brehm, J. Gmehling, H. Hofmann, U. Onken, and A. Renken), Wiley-VCH Verlag GmbH, Weinheim, pp. 195–226.
28. Baerns, M., Hinrichsen, K.-O., Hofmann, H., and Renken, A. (2013) in *Chemische Reaktionstechnik. Technische Chemie* (eds M. Baerns, A. Behr, A. Brehm, *et al.*), Wiley-VCH Verlag GmbH, Weinheim, 736 p.
29. Böwing, A.G., Jess, A., and Wasserscheid, P., Kinetics and reaction engineering of the synthesis of ionic liquids. (Kinetik und Reaktionstechnik der Synthese ionischer Flüssigkeite). *Chem. Ing. Tech.*, 2005. **77** (9): 1430–1439.
30. Renken, A., Hessel, V., Lob, P., Miszczuk, R., Uerdingen, M., and Kiwi-Minsker, L. (2007) Ionic liquid synthesis in a microstructured reactor for process intensification. *Chem. Eng. Process.*, **46**, 840–845.
31. Jacquemin, J., Husson, P., Padua, A.A.H., and Majer, V. (2006) Density and viscosity of several pure and water-saturated ionic liquids. *Green Chem.*, **8** (2), 172–180.
32. Ficke, L.E., Rodríguez, H.C., and Brennecke, J.F. (2008) Heat capacities and excess enthalpies of 1-ethyl-3-methylimidazolium-based ionic liquids and water. *J. Chem. Eng. Data*, **53** (9), 2112–2119.
33. Ge, R., Hardacre, C., Nancarrow, P., and Rooney, D.W. (2007) Thermal conductivities of ionic liquids over the temperature range from 293 K to 353 K. *J. Chem. Eng. Data*, **52** (5), 1819–1823.
34. Barthe, P., Guermeur, C., Lobet, O., Moreno, M., Woehl, P., Roberge, D.M., Bieler, N., and Zimmermann, B. (2008) Continuous multi-injection reactor for multipurpose production – part I. *Chem. Eng. Technol.*, **31** (8), 1146–1154.
35. Haber, J., Kashid, M.N., Renken, A., and Kiwi-Minsker, L. (2011) Heat management in single and multi-injection microstructured reactors: scaling effects, stability analysis, and role of mixing. *Ind. Eng. Chem. Res.*, **51** (4), 1474–1489.
36. Löwe, H., Axinte, R.D., Breuch, D., and Hofmann, C. (2009) Heat pipe controlled syntheses of ionic liquids in microstructured reactors. *Chem. Eng. J.*, **155** (1-2), 548–550.
37. Antes, J., Boskovic, D., Krause, H., Loebbecke, S., Lutz, N., Tuercke, T., and Schweikert, W. (2003) Analysis and improvement of strong exothermic nitrations in microreactors. *Chem. Eng. Res. Des.*, **81** (7), 760–765.
38. Ducry, L. and Roberge, D.M. (2008) Dibal-H reduction of methyl butyrate into butyraldehyde using microreactors. *Org. Process Res. Dev.*, **12** (2), 163–167.